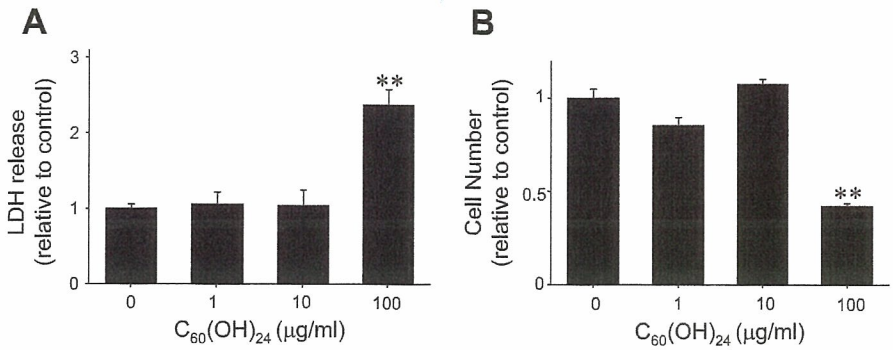

Fig. 2. Fullerene-induced cytotoxic injury in HUVECs. HUVECs at ~90% confluence were treated with $C_{60}(OH)_{24}$ (1–100 μg/ml for 24 h). Culture medium was then collected. *A*: lactate dehydrogenase (LDH) released into the supernatant was measured using a commercially available kit. Cytotoxicity was expressed relative to basal LDH release in controls (n = 4–11). *B*: living cell number was calculated using water-soluble tetrazolium salt (WST-8). n = 3; $^{**}P < 0.01$ vs. controls.

"Eukaryotic Sample and Array Processing," chapt. 1, "Eukaryotic Target Preparation"; http://www.affymetrix.com/support/technical/manuals.affx). Total RNA (2 μg) was amplified for each sample. Next, cRNA (30 μg) was fragmented in 40 μl of 1× fragmentation buffer. Hybridization cocktails were made as described in the *GeneChip Expression Analysis Technical Manual* (701021, Rev. 5, section 2, chapt. 2, "Eukaryotic Target Hybridization") and hybridized to human genome U133 plus2.0 chips at 60 rpm and 45°C for 16 h using the Hybridization Oven 640 110 V (no. 800138; Affymetrix, Santa Clara, CA). Human genome U133 plus2.0 chips (Affymetrix) comprise 54,000 probe sets and provide comprehensive coverage of the transcribed human genome on a single array to analyze expression levels of >47,000 transcripts and variants, including 38,500 well-characterized human genes plus ~6,500 new genes. GeneChips were stained with streptavidin-phycoerythrin using a Fluidics Station 450 (00-0079; Affymetrix). After being washed extensively, GeneChips were scanned using a GeneChip Scanner 3000 (00-0074; Affymetrix). Data were analyzed using GeneChip Operating Software version 1.1 (no. 690036; Affymetrix) according to GeneChip Expression Analysis Data Analysis Fundamentals (chapt. 4, "First-Order Data Analysis and Data Quality Assessment"; and chapt. 5, "Statistical Algorithms Reference"; http://www.affymetrix.com/support/technical/manuals.

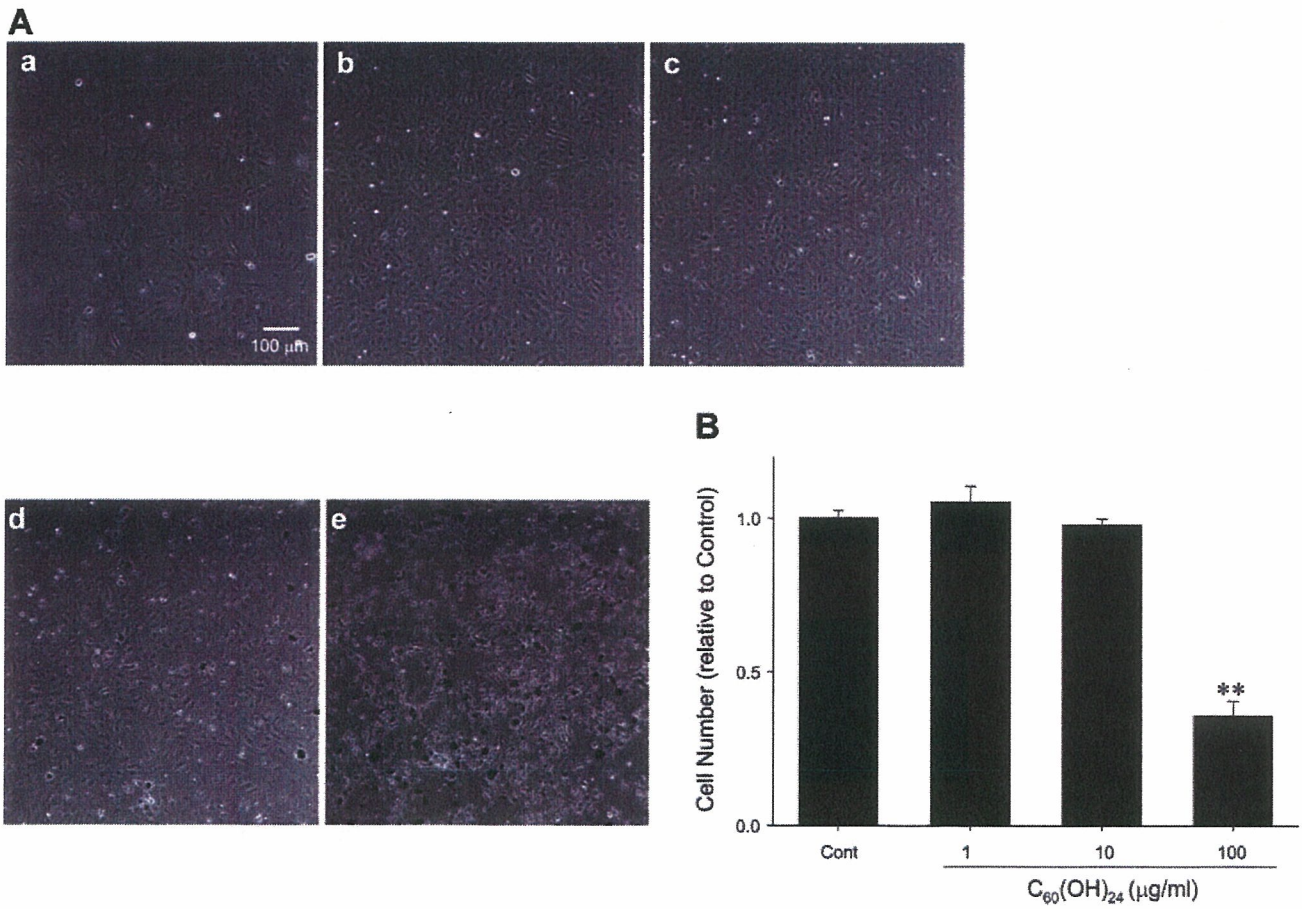

Fig. 3. Fullerene-inhibited cell growth in HUVECs. HUVECs at ~30% confluence were treated with $C_{60}(OH)_{24}$ (1–100 μg/ml) for 24 h. *A*: representative photomicrographs are shown (*a*: Start; *b*: 0 μg/ml; *c*: 1 μg/ml; *d*: 10 μg/ml; and *e*: 100 μg/ml; all for 24 h). Scale bar, 100 μm. *B*: total number of living cells was counted using WST-8. Results are shown relative to controls. n = 6; $^{**}P < 0.01$ vs. controls.

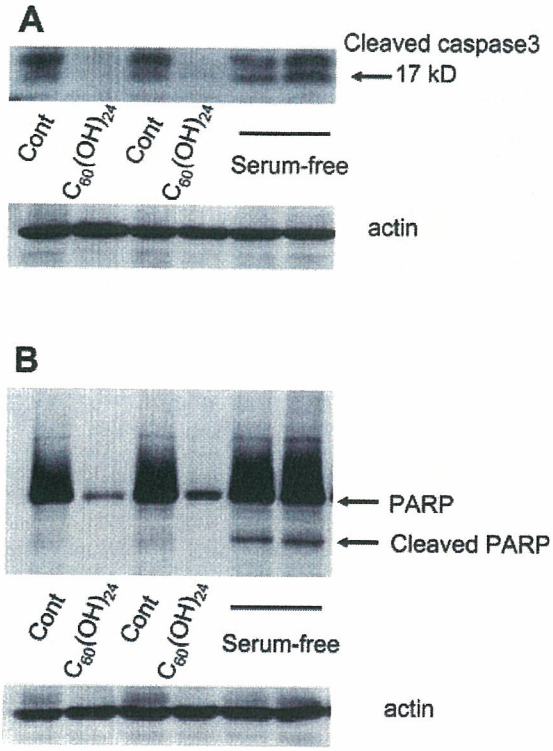

Fig. 4. Fullerene does not induce apoptosis in HUVECs. After HUVECs at ~90% confluence were treated with 100 μg/ml $C_{60}(OH)_{24}$ for 24 h, total cell lysates were harvested. Cleaved caspase-3 (17 kDa; *A*) and poly(ADP-ribose) polymerase (PARP; *B*) expression were determined using Western blot analysis. Equal protein loading was confirmed using total actin antibody.

affx). To allow comparison, all chips were scaled to a target intensity of 500 on the basis of all probe sets on each chip. Comparison of GeneChip array data was obtained using custom analysis services (Kurabo Industries, Osaka, Japan). Kurabo Industries is the authorized service provider for Affymetrix Japan (Tokyo, Japan). Genes that were significantly upregulated (top 100 genes; see Supplemental Table 1; http://ajpcell.physiology.org/cgi/content/full/00481.2005/DC1) or downregulated (top 100 genes; Supplemental Table 2) in two independent experiments are summarized. Microarray data were deposited in the National Center for Biotechnology Information's Gene Expression Omnibus (GenBank accession no. GSE3364).

Statistical analysis. Data are means ± SE. Statistical evaluations were performed using an unpaired Student's *t*-test. Values of $P < 0.05$ were considered statistically significant.

RESULTS

Fullerene induces cytotoxic morphological changes in HUVECs. To examine the direct effects on vascular ECs, cultured HUVECs were treated with $C_{60}(OH)_{24}$ for 24 h. Fullerenes (1–100 μg/ml) induced cytotoxic morphological changes in HUVECs such as vacuole formation in the cytosol and decreased cell density in a dose-dependent manner (Fig. 1, *A–D*). Figure 1, *E* (Control) and *F* [100 μg/ml $C_{60}(OH)_{24}$], represent low-magnification pictures, and cell density was clearly decreased after treatment with fullerene.

Fullerene increases release of LDH from HUVECs. To assess EC injury by fullerene quantitatively, we examined the effects of fullerenes on endothelial LDH release, a marker of cell death and injury of the plasma membrane. Although 10 μg/ml $C_{60}(OH)_{24}$ showed slight cytotoxic morphological changes (Fig. 1*C*), only the maximal concentration of $C_{60}(OH)_{24}$ (100 μg/ml, 24 h, $n = 8$) significantly increased LDH release into culture medium (Fig. 2*A*) (LDH increased 2.4 ± 0.2-fold vs. controls, $n = 11$; $P < 0.01$). To further explore the degree of cell injury after fullerene treatment, we calculated the living cell number using WST-8. A maximal dose of 100 μg/ml $C_{60}(OH)_{24}$ killed 58.0 ± 1.7% of cells ($n = 3$; $P < 0.01$ vs. controls) (Fig. 2*B*).

Fullerene has antiproliferative effects on HUVECs. To examine the effects of fullerene on cell growth, HUVECs at ~30% confluence were treated with $C_{60}(OH)_{24}$ (1–100 μg/ml) for 24 h and then the total number of living cells was measured using WST-8. HUVEC growth was inhibited by $C_{60}(OH)_{24}$ in a dose-dependent manner (Fig. 3*A*). Quantitative analysis (Fig. 3*B*) revealed that only the maximal concentration of 100 μg/ml $C_{60}(OH)_{24}$ significantly inhibited cell growth (64.2 ± 4.7%, $n = 6$; $P < 0.01$ vs. controls).

Fullerene does not induce apoptosis in HUVECs. We next examined whether fullerene induces apoptosis in vascular ECs. Serum starvation but not a maximal dose of $C_{60}(OH)_{24}$ (100 μg/ml, 24 h) induced cleavage of caspase-3 (17 kDa) and PARP (Fig. 4), which are markers for the activation of the apoptotic cascade (5, 20). This suggests that fullerene does not induce apoptosis in HUVECs. Notably, protein bands for both

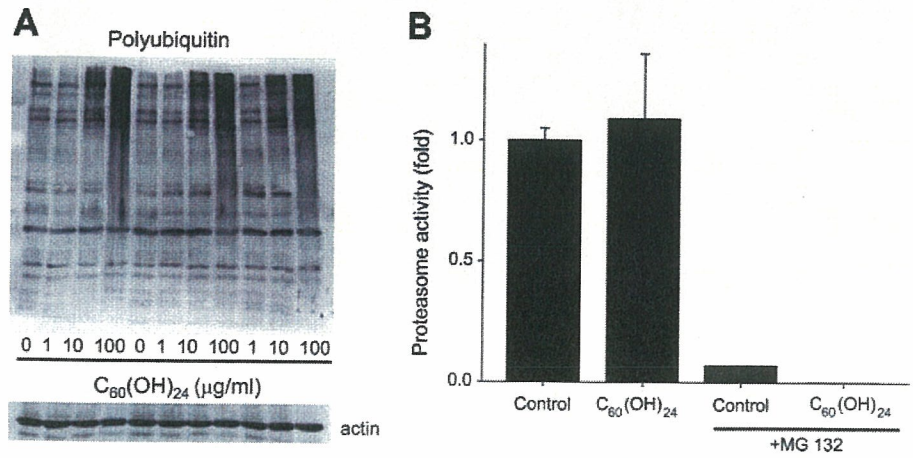

Fig. 5. Fullerene treatment induces polyubiquitination in HUVECs. After HUVECs at ~90% confluence were treated with $C_{60}(OH)_{24}$ (1–100 μg/ml) for 24 h, total cell lysates were harvested. *A*: accumulation of polyubiquitin was determined using Western blot analysis. Equal protein loading was confirmed using total actin antibody ($n = 8$). *B*: activity of the 20S proteasome was determined using a commercially available kit. Activity of 20S proteasomes was measured on the basis of fluorescence of liberated amino-4-methylcoumarin (AMC) using excitation and emission wavelengths at 340 and 450 nm. Results shown are relative to controls ($n = 3$).

caspase-3 and PARP were weak in $C_{60}(OH)_{24}$-treated samples. This finding is consistent with fullerene-treated samples in other immunoblot analysis experiments. We speculate that this phenomenon is due to protein degeneration by fullerene.

Fullerene induces accumulation of polyubiquitinated proteins in HUVECs. Because activation of the ubiquitin-proteasome system represents another death pathway, protein polyubiquitination by fullerene was examined. $C_{60}(OH)_{24}$ (1–100 μg/ml, 24 h, $n = 8$) induced protein polyubiquitination in a dose-dependent manner (Fig. 5*A*). Proteasome activity assay showed that 100 μg/ml $C_{60}(OH)_{24}$ (24 h) did not directly modify it (Fig. 5*B*) (1.09 ± 0.27-fold increase vs. controls; $n = 3$). Proteasome activity in cell lysates was suppressed almost completely by a proteasome inhibitor, MG132 (1 μM).

Ultrastructural features of HUVECs: fullerene facilitates autophagic cell death. We next performed ultrastructural analysis using transmission electron microscopy. The cytoplasm of untreated HUVECs (control) (Fig. 6*A*) contained small vesicles. In vascular smooth muscle cells, the formation of small vesicles reportedly occurs under normal physiological conditions to remove abnormal proteins and cytoplasmic macromolecules (15). Treatment of HUVECs with the maximal dose of $C_{60}(OH)_{24}$ (100 μg/ml, 24 h) caused extensive vacuolization and internalization of fullerene (Fig. 6*B*). Fullerene aggregates were observed primarily within autophagosome-like vesicles (Fig. 6, *C* and *D*). To show that vesicles represented autophagosomes, Western blot analysis was performed to detect LC3 II because conversion of LC3 I (cytosolic isoform) to LC3 II (membrane-bound form) are frequently used markers for autophagosomes (9, 32). Figure 7 clearly shows that 100 μg/ml $C_{60}(OH)_{24}$ (24 h) increased levels of the LC3 II isoform ($n = 4$).

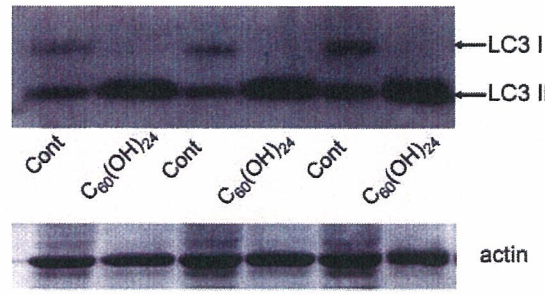

Fig. 7. Fullerene induced the formation of autophagosomes in HUVECs. After HUVECs at ~90% confluence were treated with 100 μg/ml $C_{60}(OH)_{24}$ for 24 h, total cell lysates were harvested. Autophagosomes were detected using Western blot analysis with light chain (LC)3 antibody ($n = 4$). *Top band* represents cytosolic LC3 I, and *bottom band* represents membrane-bound LC3 II, a typical marker for autophagosomes. Equal protein loading was confirmed using total actin antibody.

Chronic effects of low-dose fullerene on EC toxicity. We examined the chronic effects of low concentrations of $C_{60}(OH)_{24}$ (1–10 μg/ml, up to 10 days) on EC toxicity. During this time, cells were subcultured three times (*passages 3–6*). Media containing fullerene were changed every 2 days. Chronic treatment with 1 μg/ml $C_{60}(OH)_{24}$ for 10 days had no significant effects on EC toxicity (data not shown). Figure 8 shows the morphological features of HUVECs treated without (control) or with 10 μg/ml $C_{60}(OH)_{24}$. Fullerene was treated soon after splitting cells from *passages 3* to *4*. On *day 2*, both control and fullerene-treated cells reached subconfluence, but fullerene-treated cells showed clear morphological changes such as cytosolic vacuole formation and spindlelike cell shape.

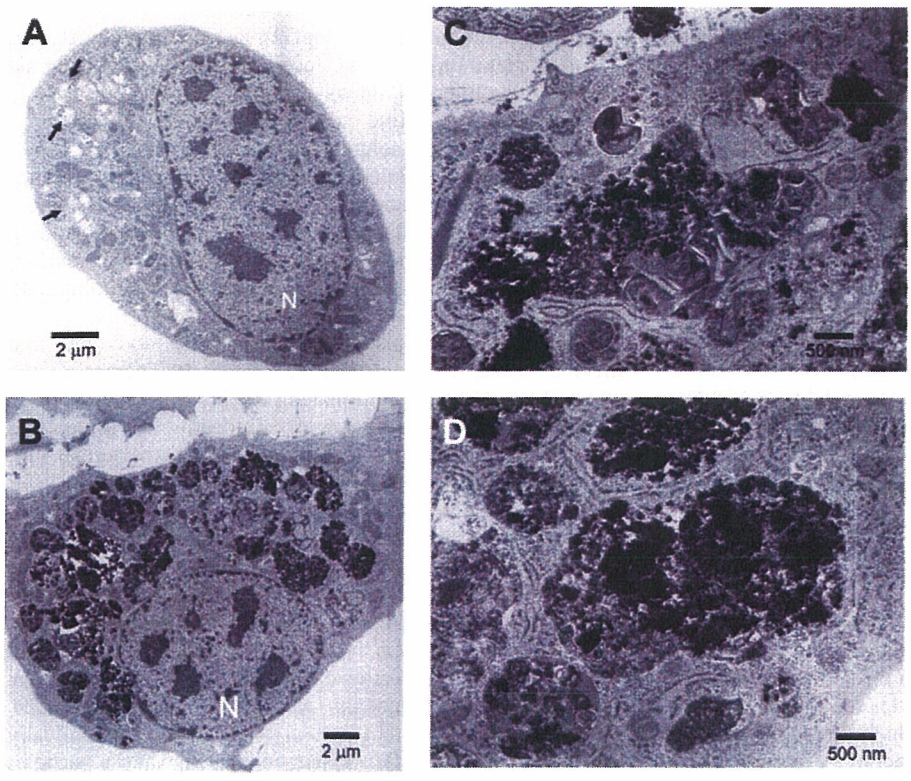

Fig. 6. Ultrastructural features of HUVECs treated with $C_{60}(OH)_{24}$. HUVECs were treated without (*A*; control) or with 100 μg/ml $C_{60}(OH)_{24}$ (*B–D*) for 24 h. N, nucleus. Arrows indicate vacuoles with phagocytotic function. Scale bars, 2 μm (*A* and *B*) and 500 nm (*C* and *D*).

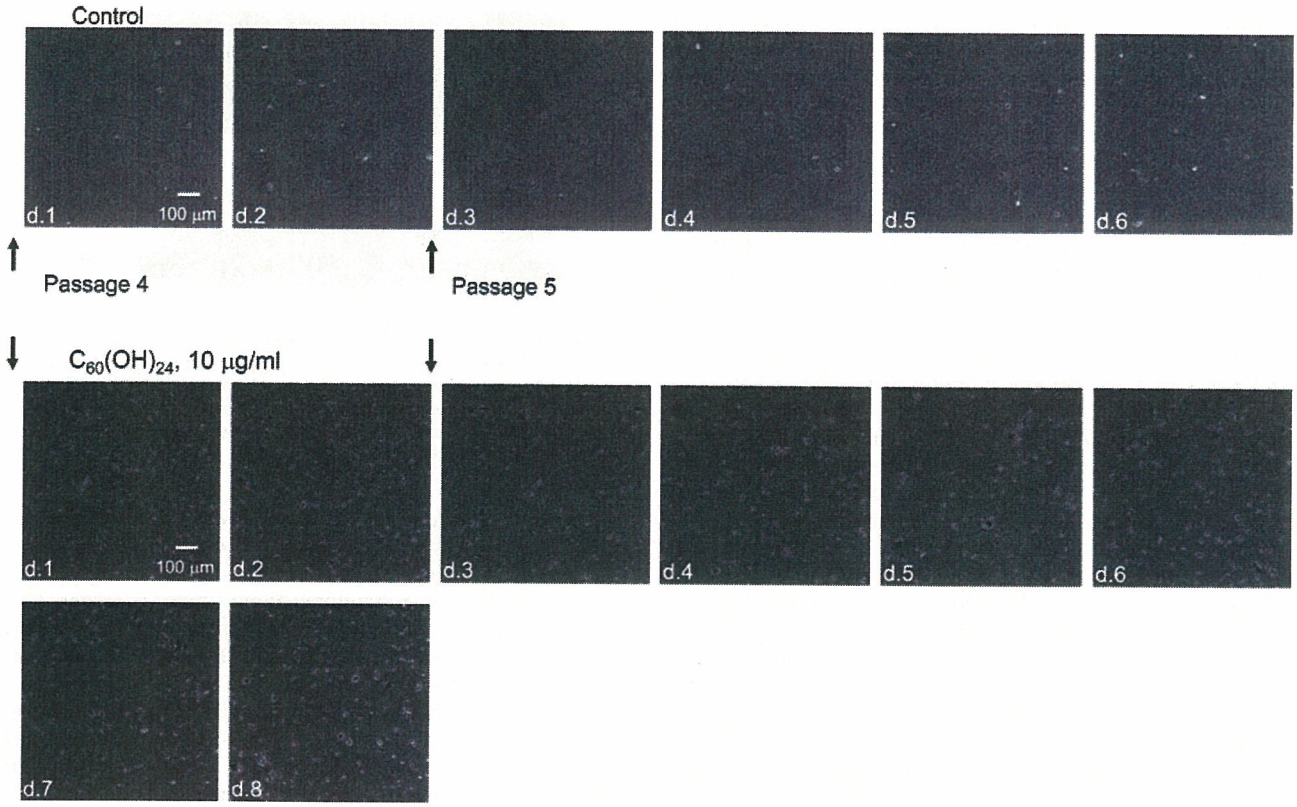

Fig. 8. Chronic effects of low-dose fullerene on HUVECs. HUVECs were treated without (Control) or with 10 μg/ml $C_{60}(OH)_{24}$ for 8 days. Cells from *passages 4* and *5* were used. Treatment was started soon after splitting cells from *passages 3* and *4*. Culture media containing fullerene were changed every 2 days. Representative morphological features are shown. Scale bar, 100 μm. Arrows indicate time of splitting.

After the second passage, control cells reached confluence within 4 days. In contrast, the attachment of cells (*day 3*) was bad in fullerene-treated groups and cell growth speed was slow. On *day 8*, fullerene-treated cells reached confluence, but the shapes of the cells were bad (spindlelike) and vacuole formation was commonly observed, suggesting the possibility that fullerene-resistant types of cells survived and increased.

Microarray analysis. Finally, microarray analysis was performed using total RNA from HUVECs treated with the maximal dose of $C_{60}(OH)_{24}$ (100 μg/ml, 24 h). Results from 2 independent samples are summarized in Supplemental Tables 1 and 2. Of note, although these were not top 100 genes, several genes related to the ubiquitin-proteasome system were significantly upregulated by fullerene [HECT (a COOH-terminal catalytic homologous to E6-AP-COOH terminus domain), C2, and WW domain containing E3 ubiquitin protein ligase 2 (ratio, 2.3 to 1), ubiquitin-specific protease 31 (ratio, 1.7 to 1), ubiquitin-specific protease 32 (ratio, 1.7 to 1), and ubiquitin-conjugating enzyme E2 (ratio, 1.5 to 1)].

DISCUSSION

The major findings of the present study are that water-soluble fullerene directly affects vascular ECs to cause cytotoxic injury or cell death and inhibition of cell growth. To the best of our knowledge, this study provides the first demonstration of the direct effects of water-soluble fullerene on vascular endothelium. In other human cells, including dermal fibroblasts, liver carcinoma cells (HepG2), neuronal astrocytes, and T-lymphocytes (Jurkat cells), recent reports have noted that water-soluble fullerene shows cytotoxic effects, presumably via production of reactive oxygen species (22, 24). Notably, several types of water-soluble fullerene derivatives are available [e.g., hydroxyl fullerene used herein, dendritic C_{60} monoadduct (22), malonic acid C_{60} (22) and nano-C_{60} (24) (basically pristine C_{60})], and cytotoxicity to cells varies depending on the fullerene subtype used, presumably because of surfactant chemistry, including a balance between hydrophobicity and hydrophilicity (3).

Some novel mechanistic insights of this study are that fullerene causes EC injury or cell death by increasing the accumulation of polyubiquitinated proteins in the cytosol and facilitating excessive autophagic cell death. EC injury and death are closely related to the initiation of atherosclerosis (14, 23). Furthermore, through nitric oxide production, ECs offer important protective functions against ischemic heart disease, including myocardial infarction, by inhibiting platelet aggregation (16) and lowering blood pressure (27). We thus propose that exposure to nanomaterials is a potential risk for cardiovascular disease, including atherosclerosis and ischemic heart disease. However, because quantitatively significant EC toxicity from water-soluble fullerene was observed only at high dosage, further validations (particularly in vivo) are needed.

We recently found that carbon black (CB), a chemically inert carbon nanoparticle present in diesel exhaust particles

(13), shows endothelial cytotoxicity by mechanisms different from those of fullerene (31). Specifically, microarray analysis revealed that CB stimulated the induction of several proinflammatory mediators, including E-selectin, ICAM-I, IL-8, heme oxygenase-1, and prostaglandin endoperoxide synthase 2. However, such effects were not observed in fullerene-stimulated ECs. Furthermore, CB did not cause accumulation of polyubiquitinated proteins in ECs. Although the underlying mechanisms remain unclear, our findings indicate that the results reported herein could be specific to fullerene. Another report (21) examined the effects of several nanomaterials, including metals (TiO_2, SiO_2, Co, Ni, polyvinyl chloride), on endothelial toxicity. The report showed that only Co^{2+} particles possessed cytotoxic effects on ECs, supporting the concept that cytotoxicity varies among different nanoparticles.

Several pathways lead to cell death (6). Two major types of programmed cell death have been distinguished: the caspase-mediated process of apoptosis and the caspase-independent process involving autophagy.

In the present study, we found that exposure to fullerene did not induce cleavage of caspase-3 or PARP, which are the hallmarks of apoptosis (5, 20). Furthermore, no clear chromatin condensation was apparent in the nuclei (Fig. 6*B*). The present results thus indicate that the induction of apoptosis does not seem to be responsible for fullerene-induced cell death and/or injury.

Conversely, fullerene markedly increased the accumulation of polyubiquitinated proteins (Fig. 5*A*). Normally, under physiological conditions, cells degrade ubiquitinated proteins using 20S proteasomes. Fullerene does not seem to modify proteasome activity directly (Fig. 5*B*). Ultrastructural analysis revealed the excess formation of phagosome-like vesicles in the cytosol (Fig. 6*B*). Vesicles have been determined to be autophagosomes on the basis of Western blot analysis using specific marker LC3 II (9, 32) (Fig. 7). Similarly, the formation of phagosomes was observed after treating alveolar macrophages with single-wall and multiwall carbon nanotubes (8). Autophagy (type II programmed death) is known to be an alternative pathway to exclude unnecessary proteins and cellular organelles. We thus propose that accumulation of ubiquitinated proteins and abnormal activation of an autophagic death pathway could be responsible at least for cell death or injury caused by water-soluble fullerene.

EC injury and/or death appears to represent a primary mechanism for the initiation of atherosclerosis (14, 23). Injury and/or denudation of ECs trigger the attachment of leukocytes to the subendothelial region and promote transendothelial migration of cells, allowing the initiation of atherosclerosis. EC injury also leads to the loss of beneficial functions, including antithrombogenic and blood pressure-lowering functions via nitric oxide, which leads to the progression of ischemic heart disease, including myocardial infarction. In addition to cell death and injury, fullerene also inhibited EC growth. Impairment of EC growth may be related to impairment of angiogenesis. Because angiogenesis is crucial to the maintenance of vascular integrity by forming collateral vessels in response to tissue ischemia (11), fullerene inhibition of EC growth may be related to the progression of ischemic heart disease. Collectively, the present findings support the concept that exposure to fullerene could be a risk for atherosclerosis and ischemic heart disease.

The present study used 1–100 μg/ml fullerene concentrations for in vitro experiments. The pathophysiological concentrations of fullerene are barely known. In addition to engineered nanomaterials, traffic-derived nanoparticles are known to represent a risk for cardiovascular disorders, including atherosclerosis and ischemic heart disease (2, 4). The maximal concentration of particulate matter <2.5 μm in Chongqing, one of the biggest cities in China, was ~700 $\mu g/m^3$ (daily average) (26), indicating that an individual could inhale ~10,000 μg of particulate matter during the course of 24 h there. This value is equivalent to ~1 μg/ml when the extracellular fluid volume is 12 L in a 60-kg person. The fullerene dosage used in this study was up to 100-fold higher than this level.

The kinetics of water-soluble fullerene in vivo have not yet been completely determined. Normally, inhaled microparticles are cleaned off by alveolar macrophages via phagocytosis. However, this is not applicable to nanoparticles (2, 19), which appear to translocate to extrapulmonary sites via blood and lymph and thus reach other tissues (19). Using radiolabeled water-soluble fullerene administered intravenously to rats, Yamago et al. (28) demonstrated that most fullerenes moved rapidly to the liver (within 1 h) and then were distributed to various other tissues, including spleen, lung, kidney, heart, and brain. Extraction seems slow, and >90% was retained in the body 1 wk later, raising concern about chronic toxic effects. Although we could not clearly observe EC cytotoxicity after acute treatment with low-dose fullerene (10 μg/ml, 24 h), treatment for 8 days seems to enhance toxicity (Fig. 8). The effects of chronic exposure to low-dose fullerene in vivo need to be examined, particularly with regard to the cardiovascular system.

In summary, in the present study, we examined the direct effects of water-soluble fullerene on vascular endothelial cells to explore the potential toxicity of fullerene in humans, especially regarding the cardiovascular systems. We found that fullerene causes cytotoxic injury or cell death in vascular ECs, indicating that exposure to fullerene could represent a risk for atherosclerosis and ischemic heart disease. Because cytotoxicity by water-soluble fullerene occurs only at high doses, further validation experiments using blood vessels and animal models are warranted.

ACKNOWLEDGMENTS

We are grateful to Dr. T. Yoshimori (National Institute of Genetics, Mishima, Japan) for providing LC3 antibody.

GRANTS

This study was supported by Health and Labor Sciences Research Grant for Research on Risk of Chemical Substance Grant H17-Chemistry-008 (to N. Iwai) and Grant-in-Aid for Scientific Research Grant 17790176 (to H. Yamawaki) from the Ministry of Education, Culture, Sports, Science, and Technology, Japan.

REFERENCES

1. **Åkerman ME, Chan WCW, Laakkonen P, Bhatia SN, and Ruoslahti E.** Nanocrystal targeting in vivo. *Proc Natl Acad Sci USA* 99: 12617–12621, 2002.
2. **Borm PJA and Kreyling W.** Toxicological hazards of inhaled nanoparticles: potential implications for drug delivery. *J Nanosci Nanotechnol* 4: 521–531, 2004.
3. **Bosi S, Feruglio L, Da Ros T, Spalluto G, Gregoretti B, Terdoslavich M, Decorti G, Passamonti S, Moro S, and Prato M.** Hemolytic effects of water-soluble fullerene derivatives. *J Med Chem* 47: 6711–6715, 2004.

4. **Brook RD, Franklin B, Cascio W, Hong Y, Howard G, Lipsett M, Luepker R, Mittleman M, Samet J, Smith SC Jr, and Tager I.** Air pollution and cardiovascular disease: a statement for healthcare professionals from the Expert Panel on Population and Prevention Science of the American Heart Association. *Circulation* 109: 2655–2671, 2004.
5. **Budihardjo I, Oliver H, Lutter M, Luo X, and Wang X.** Biochemical pathways of caspase activation during apoptosis. *Annu Rev Cell Dev Biol* 15: 269–290, 1999.
6. **Clarke PG.** Developmental cell death: morphological diversity and multiple mechanisms. *Anat Embryol (Berl)* 181: 195–213, 1990.
7. **Colvin VL.** The potential environmental impact of engineered nanomaterials. *Nat Biotechnol* 21: 1166–1170, 2003.
8. **Jia G, Wang H, Yan L, Wang X, Pei R, Yan T, Zhao Y, and Guo X.** Cytotoxicity of carbon nanomaterials: single-wall nanotube, multi-wall nanotube, and fullerene. *Environ Sci Technol* 39: 1378–1383, 2005.
9. **Kabeya Y, Mizushima N, Ueno T, Yamamoto A, Kirisako T, Noda T, Kominami E, Ohsumi Y, and Yoshimori T.** LC3, a mammalian homologue of yeast Apg8p, is localized in autophagosome membranes after processing. *EMBO J* 19: 5720–5728, 2000.
10. **Katsouyanni K, Touloumi G, Samoli E, Gryparis A, Le Tertre A, Monopolis Y, Rossi G, Zmirou D, Ballester F, Boumghar A, Anderson HR, Wojtyniak B, Paldy A, Braunstein R, Pekkanen J, Schindler C, and Schwartz J.** Confounding and effect modification in the short-term effects of ambient particles on total mortality: results from 29 European cities within the APHEA2 project. *Epidemiology* 12: 521–531, 2001.
11. **Kondo T, Kobayashi K, and Murohara T.** Nitric oxide signaling during myocardial angiogenesis. *Mol Cell Biochem* 264: 25–34, 2004.
12. **Kreuter J.** Nanoparticulate systems for brain delivery of drugs. *Adv Drug Deliv Rev* 47: 65–81, 2001.
13. **Lam CW, James JT, McCluskey R, and Hunter RL.** Pulmonary toxicity of single-wall carbon nanotubes in mice 7 and 90 days after intratracheal instillation. *Toxicol Sci* 77: 126–134, 2004.
14. **Libby P.** Inflammation in atherosclerosis. *Nature* 420: 868–874, 2002.
15. **Martinet W, De Bie M, Schrijvers DM, De Meyer GR, Herman AG, and Kockx MM.** 7-Ketocholesterol induces protein ubiquitination, myelin figure formation, and light chain 3 processing in vascular smooth muscle cells. *Arterioscler Thromb Vasc Biol* 24: 2296–2301, 2004.
16. **Moncada S, Palmer RM, and Higgs EA.** Nitric oxide: physiology pathophysiology, and pharmacology. *Pharmacol Rev* 43: 109–142, 1991.
17. **Nemmar A, Hoet PH, Vanquickenborne B, Dinsdale D, Thomeer M, Hoylaerts MF, Vanbilloen H, Mortelmans L, and Nemery B.** Passage of inhaled particles into the blood circulation in humans. *Circulation* 105: 411–414, 2002.
18. **Nemmar A, Hoylaerts MF, Hoet PH, and Nemery B.** Possible mechanisms of the cardiovascular effects of inhaled particles: systemic translocation and prothrombotic effects. *Toxicol Lett* 149: 243–253, 2004.
19. **Oberdorster G, Oberdorster E, and Oberdorster J.** Nanotoxicology: an emerging discipline evolving from studies of ultrafine particles. *Environ Health Perspect* 113: 823–839, 2005.
20. **Patel T, Gores GJ, and Kaufmann SH.** The role of proteases during apoptosis. *FASEB J* 10: 587–597, 1996.
21. **Peters K, Unger RE, Kirkpatrick CJ, Gatti AM, and Monari E.** Effects of nano-scaled particles on endothelial cell function in vitro: studies on viability, proliferation and inflammation. *J Mater Sci Mater Med* 15: 321–325, 2004.
22. **Rancan F, Rosan S, Boehm F, Cantrell A, Brellreich M, Schoenberger H, Hirsch A, and Moussa F.** Cytotoxicity and photocytotoxicity of a dendritic C_{60} mono-adduct and a malonic acid C_{60} tris-adduct on Jurkat cells. *J Photochem Photobiol B* 67: 157–162, 2002.
23. **Ross R.** Atherosclerosis: an inflammatory disease. *N Engl J Med* 340: 115–126, 1999.
24. **Sayes CM, Gobin AM, Ausman KD, Mendez J, West JL, and Colvin VL.** Nano-C_{60} cytotoxicity is due to lipid peroxidation. *Biomaterials* 26: 7587–7595, 2005.
25. **Seaton A and Donaldson K.** Nanoscience, nanotoxicology, and the need to think small. *Lancet* 365: 923–924, 2005.
26. **Venners SA, Wang B, Xu Z, Schlatter Y, Wang L, and Xu X.** Particulate matter, sulfur dioxide, and daily mortality in Chongqing, China. *Environ Health Perspect* 111: 562–567, 2003.
27. **Wilkinson IB, Franklin SS, and Cockcroft JR.** Nitric oxide and the regulation of large artery stiffness: from physiology to pharmacology. *Hypertension* 44: 112–116, 2004.
28. **Yamago S, Tokuyama H, Nakamura E, Kikuchi K, Kananishi S, Sueki K, Nakahara H, Enomoto S, and Ambe F.** In vivo biological behavior of a water-miscible fullerene: [^{14}C] labeling, absorption, distribution, excretion and acute toxicity. *Chem Biol* 2: 385–389, 1995.
29. **Yamawaki H, Lehoux S, and Berk BC.** Chronic physiological shear stress inhibits tumor necrosis factor-induced proinflammatory responses in rabbit aorta perfused ex vivo. *Circulation* 108: 1619–1625, 2003.
30. **Yamawaki H, Pan S, Lee RT, and Berk BC.** Fluid shear stress inhibits vascular inflammation by decreasing thioredoxin-interacting protein in endothelial cells. *J Clin Invest* 115: 733–738, 2005.
31. **Yamawaki H and Iwai N.** Mechanisms underlying nano-sized air pollution-mediated progression of atherosclerosis: carbon black causes cytotoxic injury/inflammation and inhibits cell growth in vascular endothelial cells. *Circ J* 70: 129–140, 2006.
32. **Yoshimori T.** Autophagy: a regulated bulk degradation process inside cells. *Biochem Biophys Res Commun* 313: 453–458, 2004.

[Environmental Health and Preventive Medicine 11, 292–297, November 2006]

Original Article

Genotoxicity in Cell Lines Induced by Chronic Exposure to Water-Soluble Fullerenes Using Micronucleus Test

Yasuharu NIWA[1] and Naoharu IWAI[1]

[1]*Department of Epidemiology, Research Institute, National Cardiovascular Center, Osaka, Japan*

Abstract

Objectives: Nanomaterials have numerous potential benefits for society, but the effects of nanomaterials on human health are poorly understood. In this study, we aim to determine the genotoxic effects of chronic exposure to nanomaterials in various cell lines.

Methods: Chinese hamster ovary (CHO) cells, human epidermoid-like carcinoma (Hela) cells and human embryonic kidney 293 (HEK293) cells were treated with the water-soluble fullerene $C_{60}(OH)_{24}$ for 33–80 days. Cell proliferation, cytotoxic analysis and micronucleus tests were performed.

Results: When treated with $C_{60}(OH)_{24}$ (0, 10, 100, or 1000 pg/ml) for 33 days, both the HEK293 and Hela cells showed increased cell proliferation, but cellular lactate dehydrogenase (LDH) activity was not affected. After long-term exposure (80 days) to $C_{60}(OH)_{24}$ (0, 10, 100, or 1000 pg/ml), the CHO, Hela and HEK293 cells showed increased genotoxicity on the micronucleus test.

Conclusion: This study suggests that nanomaterials, such as $C_{60}(OH)_{24}$, have genotoxic effects.

Key words: water-soluble fullerene, genotoxicity, micronucleus test

Introduction

Environmental health studies have focused on the relationship between health outcome and ambient levels of PM10 and PM2.5, which are particles having aerodynamic diameters <10 and 2.5 μm, respectively. Recently, however, epidemiological studies have begun focusing on ultrafine particles (UFPs) having a diameter of <100 nm, which are abundant but account for a small proportion of total particle mass. UFPs are important with regard to adverse health effects due to their high alveolar deposition fraction (1–3).

Biomedical applications under development include targeted drug delivery systems for brain and tumor tissues, as well as intravascular nanosensor and nanorobotic devices for imaging and diagnosis. However, the potential adverse effects or humeral response following the introduction of nanomaterials into an organism remain unknown (4–6). After inhaled nanomaterials are deposited in the respiratory tract, their small size allows cellular uptake and transcytosis into the vascular and lymphatic systems.

Received Jun. 12, 2006/Accepted Aug. 30, 2006
Reprint requests to: Yasuharu NIWA, PhD
Department of Epidemiology, Research Institute, National Cardiovascular Center, Suita, Osaka 565-8565, Japan
TEL: +81(6)6833-5012, FAX: +81(6)6835-2088
E-mail: yniwa@ri.ncvc.go.jp

Our experiments have demonstrated that both carbon black (CB) and water-soluble fullerene [$C_{60}(OH)_{24}$] exhibit cytotoxicities, such as decreased cell density and cell growth, and that CB facilitates autophagic cell death in human umbilical vein endothelial cells. Furthermore, CB and $C_{60}(OH)_{24}$ up-regulate the expression of inflammation- and ubiquitin-proteasome-related genes, indicating that exposure to CB or $C_{60}(OH)_{24}$ represents a risk of atherosclerosis and ischemic heart disease (7, 8).

The results of epidemiologic and animal studies have suggested that exposure to nanoparticles plays roles in cardiovascular diseases such as atherosclerosis and myocardial infarction (2, 3, 9–12), and in genetic damage to cells or tissues (13–16). However, how exposure to airborne particulate matter induces genetic changes in germ lines or tissues is poorly understood. The small size of nanoparticles may allow them to be inhaled into the respiratory system, where they can pass into the bloodstream, ultimately reaching the germ lines. Nanomaterials then have the potential to adversely affect these cells.

Nanomaterial cytotoxicity in cells varies with chemical characteristics and surface properties, including hydrohobicity, hydrophilicity, and surface area per molecule (1, 5). Experimental studies have shown that $C_{60}(OH)_{24}$ may stimulate reactive oxygen species production in cells or tissues, and may inhibit cell proliferation or induce cell death (14). In contrast, other experimental studies have shown that $C_{60}(OH)_{24}$ may scavenge produced reactive oxygen species, and inhibit cell proliferation (17). The aim of the this study is to investigate the cytotoxic

and genotoxic effects of long-term exposure to $C_{60}(OH)_{24}$ in cultured cells. In particular, we focused on genotoxicity in germ cell [Chinese hamster ovary (CHO) cells: short G1 phase], somatic cell [human embryonic kidney 293 (HEK293) cells], and adult cell [human epidermoid-like carcinoma cells (Hela) cells: long period of G1 phase] models.

Materials and Methods

Materials

Hydroxyl fullerene {$C_{60}(OH)_{24}$; Tokyo Progress System, Tokyo, Japan} was used as described (7, 8), and its diameter was 7.1±2.4 nm.

Cell culture

All cell lines (CHO, Hela, HEK293) were obtained from Dainippon Seiyaku (Osaka, Japan) and were cultured in DMEM with 10% fetal bovine serum (Hyclone, Utah, USA). In experiments, cells were cultured in DMEM with 2% FBS and sonicated $C_{60}(OH)_{24}$ (0, 10, 100, or 1000 pg/ml or 20, 100 ng/ml). Cells were passaged every 3–4 days. Representative photomicrographs of CHO, Hela and HEK293 cells treated with $C_{60}(OH)_{24}$ had taken. CHO, Hela and HEK293 cells at ~30% confluence were treated with $C_{60}(OH)_{24}$ (0, 20, or 100 ng/ml) for 3 or 6 days.

LDH assay

Lactate dehydrogenase (LDH) activity was analyzed using a CytoTox 96 nonradioactive cytotoxicity assay kit (Promega, Madison, WI) in accordance with the manufacturer's protocols. Cells at 50–60% confluence were treated with $C_{60}(OH)_{24}$ for 33 days. LDH activity in the culture medium was evaluated on the basis of absorbance at 490 nm using a microplate reader (ARVO; PerkinElmer, Japan). Cytotoxicity was expressed relative to basal LDH release rate in untreated cells.

Proliferation assay

Cell proliferation assay was performed using a Cell Counting-8 kit (Dojindo laboratories, Kumamoto, Japan) in accordance with the manufacturer's protocols. Cells were cultured in 12-well plates and treated with $C_{60}(OH)_{24}$ (0, 10, 100, or 1000 pg/ml) for 33 days. An assay solution was added in each well, and after incubating for 3 h, the media were transferred to 96-well plates. Cell growth was measured on the basis of absorbance at 450 nm using an ARVO microplate reader.

Micronucleus test

A micronucleus test was performed in accordance with the method of Matsushima et al. (18), with slight modifications. Cells were cultured in six-well plates for 24 h, and then exposed to $C_{60}(OH)_{24}$ (0, 10, 100, or 1000 pg/ml) for 80 days. After exposure to $C_{60}(OH)_{24}$, the cells were washed 3 times with PBS, and suspended in a hypotonic solution (75 mM KCl) for 10 min at room temperature. The cells were then resuspended in cold methanol containing 25% acetic acid. After fixation, the cells were then suspended in methanol containing 1% acetic acid and spotted onto a glass slide. The cells were then air-dried and mounted with 4',6-diamido-2-phenyindole dilactate (DAPI)-containing medium. The nucleus was observed under a fluorometry microscope at 200× magnification. The number of micronucleated cells per 1000 cells was determined.

Statistical analysis

Data are presented as mean±SEM. Statistical evaluation was performed using an unpaired Student's t test. p values of <0.05 were considered to be statistically significant.

Results

We first analyzed the acute effects of exposure to relatively high doses of $C_{60}(OH)_{24}$ (0, 20, and 100 ng/ml) on cells by treating CHO, Hela and HEK293 cells with $C_{60}(OH)_{24}$ for 3 or 6 days (Fig. 1). The numbers of CHO and HEK293 cells decreased significantly in a dose-dependent manner, but the number of Hela cells did not significantly change for the 3-day exposure. The cytotoxic effects of $C_{60}(OH)_{24}$ in CHO and HEK293 cells were suppressed after 6 days; Hela cells exhibited a significantly decreased cell growth rate in a dose-dependent manner. We believe that $C_{60}(OH)_{24}$-sensitive cells died within 3 days, but $C_{60}(OH)_{24}$-resistant CHO and HEK293 cells were able to survive for 6 days. In contrast, CHO and HEK293 cells were more sensitive to ng/ml doses of $C_{60}(OH)_{24}$ than Hela cells.

To analyze the effects of very low doses of $C_{60}(OH)_{24}$ (0, 10, 100, and 1000 pg/ml), we investigated cell proliferation rate, cytotoxicity, and mitogenic effects in the three cell lines. After $C_{60}(OH)_{24}$ exposure for 33 days, the cell proliferation rates of HEK293 (peak, 1.3 fold) and Hela (peak, 2.0 fold) cells significantly increased in a dose-dependent manner (Fig. 2a). Moreover, cytotoxic effects were not observed, rather than suppressed in Hela cells under this condition (Fig. 2b). In addition, cell morphology did not change after $C_{60}(OH)_{24}$ exposure for 33 days (data not shown). These results suggest that $C_{60}(OH)_{24}$ has mitogenic rather than cytotoxic effects with long-term exposure at very low concentrations. Hela cells were more sensitive to $C_{60}(OH)_{24}$ than HEK293 cells with regard to cell growth efficiency. These results may differ owing to the cell cycle period; the G1 phase period of CHO and HEK293 cells is shorter than that of Hela cells. We hypothesized that if nanomaterials have mitogenic activity when cells are chronically exposed to $C_{60}(OH)_{24}$, abnormal nuclei such as micronuclei would be observed. After treating the cells with very low doses of $C_{60}(OH)_{24}$ for 80 days, the number of micronuclei that were stained with DAPI were determined (Fig. 3, arrowheads). The number of micronuclei was significantly higher after exposure to $C_{60}(OH)_{24}$ for 80 days than control (Fig. 4). The ratio (‰) of cells with micronuclei was also significantly high in CHO, Hela and HEK293 cells. CHO and HEK293 cells were more sensitive to $C_{60}(OH)_{24}$ than Hela cells in terms of the ratio of cells with micronuclei.

These results demonstrate that the effects of nanomaterials, such as $C_{60}(OH)_{24}$, which may have toxic, mitogenic, or mutagenetic activity, may contribute to cardiovascular diseases as well as other diseases such as cancer.

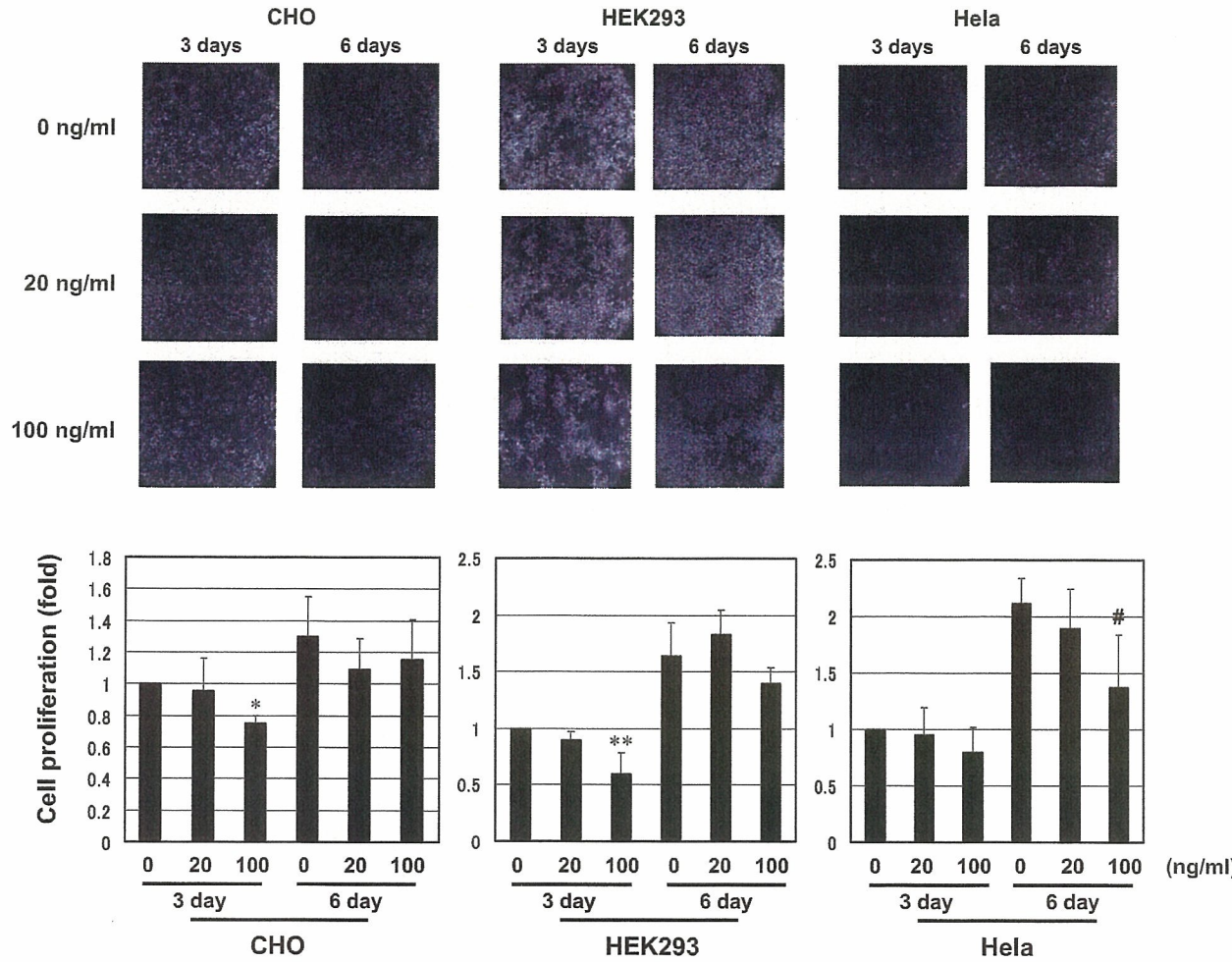

Fig. 1 Representative photomicrographs of CHO, Hela and HEK293 cells treated with $C_{60}(OH)_{24}$. CHO, Hela and HEK293 cells at ~30% confluence were treated with $C_{60}(OH)_{24}$ (0, 20, 100 ng/ml) for 3 or 6 days (upper panels). Cell number was calculated using a hemocytometer (n=4). Results are shown relative to those of controls (lower panel). * $p<0.02$, ** $p<0.03$, # $p<0.05$.

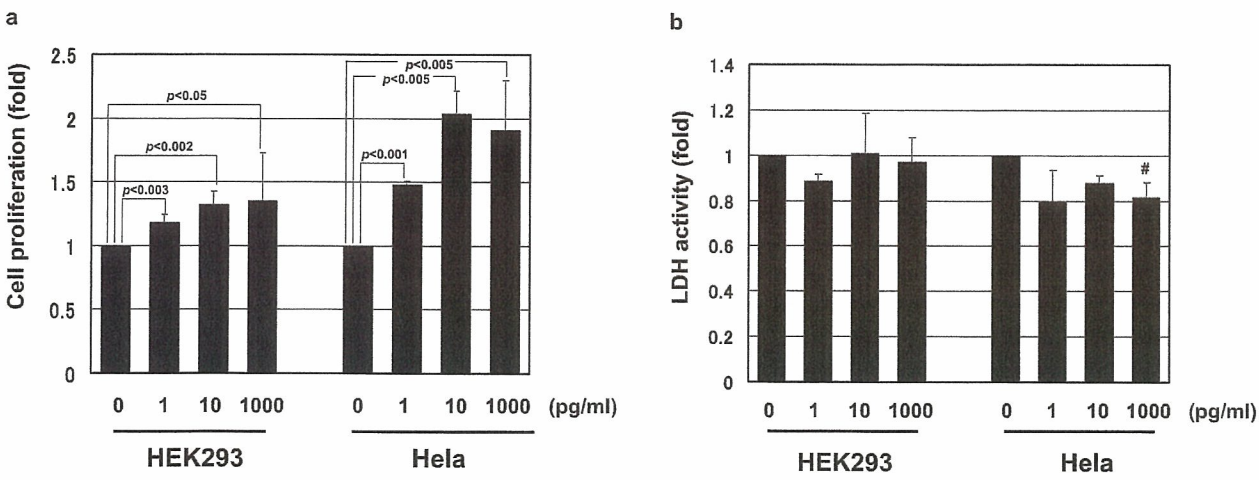

Fig. 2 $C_{60}(OH)_{24}$-induced cell growth in dose-dependent manner. HEK293 and Hela cells at ~30% confluence were treated with $C_{60}(OH)_{24}$ (0–1000 pg/ml) for 33 days. (a) The number of cells was determined using water-soluble tetrazolium salt (WST-8). (b) $C_{60}(OH)_{24}$ did not induce cytotoxic injury in HEK293 or Hela cells. Cells at ~30% confluence were treated with $C_{60}(OH)_{24}$ (0–1000 pg/ml) for 33 days. The amount of lactate dehydrogenase released into culture medium was measured. Cytotoxicity was calculated as the fold-change relative to that of the controls (n=4). Results are shown relative to those of the controls. p values indicate significance.

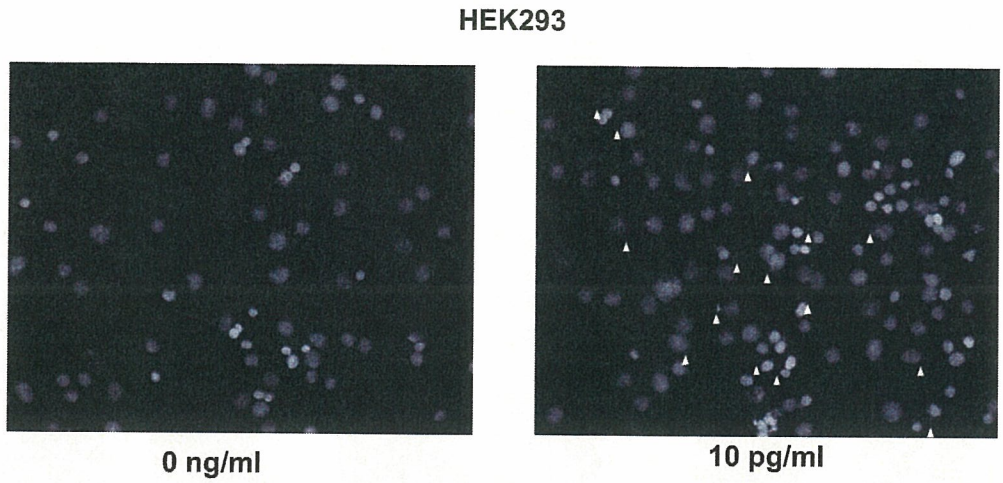

Fig. 3 The number of cells with micronuclei among HEK293 cells exposed to $C_{60}(OH)_{24}$ (0 or 10 pg/ml) for 80 days was elevated.

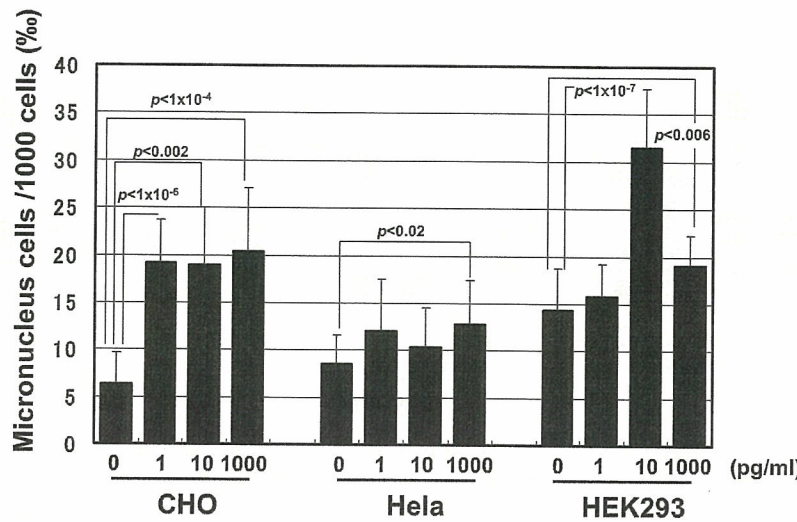

Fig. 4 Formation of micronuclei (‰) in CHO, Hela and HEK293 cells after treatment with different concentrations of $C_{60}(OH)_{24}$ for 80 days. *p* values indicate significance.

Discussion

The aim of this study is to clarify effects of chronic exposure to very low doses of nanomaterials, such as $C_{60}(OH)_{24}$, particularly with regard to genotoxicity *in vitro*. There is no evidence that pg/ml doses of $C_{60}(OH)_{24}$ have oncogenic or antioncogenic activity. Short-term exposure to relatively high doses of $C_{60}(OH)_{24}$ in the ng/ml range may induce antioncogenic functions, such as cell growth suppression (Fig. 1); however, long-term exposure to pg/ml doses of $C_{60}(OH)_{24}$ may induce cell growth (Fig. 2a). Recent studies have shown that ng/ml doses of $C_{60}(OH)_{24}$ have antioncogenic activity in various cancer cell lines (4, 19). In contrast, very low concentrations of $C_{60}(OH)_{24}$ are able to stimulate micronucleus production after long-term exposure. In this study, the cells (CHO, Hela, and HEK293) probably experienced DNA damage via an unknown mechanism (Fig. 4).

We believe that micronucleus generation caused by $C_{60}(OH)_{24}$ is not the result of chromosomal DNA damage by genotoxic molecules, such as reactive oxygen species, but is rather due to unsuccessful chromosomal DNA division during cell division during the M phase (20–22). Indeed, micronucleus production is thought to be caused when one daughter cell becomes trisomic and the other monosomic owing to aberrant segregation. The lagging chromosome may then form a micronucleus. Micronuclei can contain an entire chromosome that lags at mitosis or chromosome fragments that are not incorporated into daughter nuclei during cell division owing to kinetochore dysfunction. In addition, LDH activity was suppressed depending on the concentration of $C_{60}(OH)_{24}$ in culture medium (Fig. 2b). This shows that $C_{60}(OH)_{24}$ may scavenge reactive oxygen species, and protect against cell death. Fullerene derivatives were previously used as scavengers for reactive oxygen species, such as O_2^- and nitric oxide (17). On the basis of these results, reactive oxygen species were determined not to be involved in micronucleus generation in these experiments.

We used commercial $C_{60}(OH)_{24}$ containing about 2% (w/w) organic solvents, such as toluene. We analyzed the cytotoxic

effects of a 3-week exposure to toluene in cultured cells. At 2%, toluene did not exert any cytotoxic effects on cells (data not shown). We thus believe that $C_{60}(OH)_{24}$ stimulated a signaling pathway that influenced cell division, particularly during the period between the G2 phase and the M phase.

The results of other experiments suggest that although $C_{60}(OH)_{24}$ was used at more than 100-fold higher concentrations, both CB and $C_{60}(OH)_{24}$ induce nonapoptotic cell death mediated by the accumulation of polyubiquitinated proteins in autophagosomes, and the expression of inflammatory genes (*MCP-1*, *ICAM-1*, and *E-cadhelin*) or ubiquitin-proteasome system genes [*HECT* (a COOH-terminal catalytic homologous to E6-AP-COOH), *C2- and WW-domain-containing E3 ubiquitin protein ligase 2*, *ubiquitin-specific protease 31*, *ubiquitin-specific protease 32* and *ubiquitin-conjugating enzyme E2*] in human umbilical vein cells (7, 8). Furthermore, we demonstrated that CB and $C_{60}(OH)_{24}$ facilitate the uptake of oxidized LDL in macrophages to form foam like cells and induce the expression of the oxidized LDL receptor LOX-1 (in submission).

The kinetics of nanomaterials *in vivo* have not yet been determined. Inhaled nanoparticles are thought to be removed by alveolar macrophages via phagocytosis. By using radiolabeled water-soluble fullerene administered intravenously to rats, in which most fullerenes moved rapidly to the liver (within 1 h), it was found that fullerenes are distributed in various other tissues, including the spleen, lung, kidney, heart, and brain (23). Removal is apparently slow, with more than 90% being retained after one week, thus raising concerns about chronic toxicity. The effects of chronic exposure to nanomaterials *in vivo* thus require further examination.

Acknowledgments

This study was supported by a Health and Labor Sciences Research Grant for Research on Risk of Chemical Substance (H17-chemistry-008 to N.I.), a Grant-in-Aid for Scientific Research (#18590583 to Y.N.) from the Ministry of Education, Culture, Sports, Science, and Technology, Japan and the Program for the Promotion of Fundamental Studies in Health Science of the National Institute of Biomedical Innovation.

References

(1) Block ML, Wu X, Pei Z, Li G, Wang T, Qin L, et al. Nanometer size diesel exhaust particles are selectively toxic to dopaminergic neurons: the role of microglia, phagocytosis, and NADPH oxidase. FASEB J. 2004;18:1618–1620.

(2) Katsouyanni K, Touloumi G, Samoli E, Gryparis A, Le Tertre A, Monopolis Y, et al. Confounding and effect modification in the short-term effects of ambient particles on total mortality: results from 29 European cities within the APHEA2 project. Epidemiology. 2001;12:521–531.

(3) Nemmar A, Hoet PH, Vanquickenborne B, Dinsdale D, Thomeer M, Hoylaerts MF, et al. Passage of inhaled particles into the blood circulation in humans. Circulation. 2002;105: 411–414.

(4) Tabata Y, Murakami Y, IkadaY. Photodynamic effect of polyethylene glycol-modified fullerene on tumor. Jpn J Cancer Res. 1997;88:1108–1116.

(5) Colvin VL. The potential environmental impact of engineered nanomaterials. Nat Biotechnol. 2003;21:1166–1170.

(6) Borm PJ, Kreyling W. Toxicological hazards of inhaled nanoparticles—potential implications for drug delivery. J Nanosci Nanotechnol. 2004;4:521–531.

(7) Yamawaki H, Iwai N. Mechanisms underlying nano-sized air-pollution-mediated progression of atherosclerosis: carbon black causes cytotoxic injury/inflammation and inhibits cell growth in vascular endothelial cells. Circ J. 2006;70:129–140.

(8) Yamawaki H, Iwai N. Cytotoxicity of water-soluble fullerene in vascular endothelial cells. Am J Physiol Cell Physiol. 2006;290:C1495–1502.

(9) Dockery DW, Pope CA 3rd, Xu X, Spengler JD, Ware JH, Fay ME, et al. An association between air pollution and mortality in six U.S. cities. N Engl J Med. 1993;329:1753–1759.

(10) Peters A, Dockery DW, Muller JE, Mittleman MA. Increased particulate air pollution and the triggering of myocardial infarction. Circulation. 2001;103:2810–2815.

(11) Kodavanti UP, Moyer CF, Ledbetter AD, Schladweiler MC, Costa DL, Hauser R, et al. Inhaled environmental combustion particles cause myocardial injury in the Wistar Kyoto rat. Toxicol Sci. 2003;71:237–245.

(12) Suwa T, Hogg JC, Quinlan KB, Ohgami A, Vincent R, van Eeden SF. Particulate air pollution induces progression of atherosclerosis. J Am Coll Cardiol. 2002;39:935–942.

(13) Watts RR, Lemieux PM, Grote RA, Lowans RW, Williams RW, Brooks LR, et al. Development of source testing, analytical, and mutagenicity bioassay procedures for evaluating emissions from municipal and hospital waste combustors. Environ Health Perspect. 1992;98:227–234.

(14) Rancan F, Rosan S, Boehm K, Fernandez E, Hidalgo ME, et al. Cytotoxicity and photocytotoxicity of a dendritic C(60) mono-adduct and a malonic acid C(60) tris-adduct on Jurkat cells. J Photochem Photobiol B. 2002;67:157–162.

(15) Soares SR, Bueno-Guimaraes HM, Ferreira CM, Rivero DH, De Castro I, Garcia ML, et al. Urban air pollution induces micronuclei in peripheral erythrocytes of mice in vivo. Environ Res. 2003;92:191–196.

(16) Somers CM, McCarry BE, Malek F, Quinn JS. Reduction of particulate air pollution lowers the risk of heritable mutations in mice. Science. 2004;304:1008–1010.

(17) Mirkov SM, Djordjevic AN, Andric NL, Andric SA, Kostic TS, Bogdanovic GM, et al. Nitric oxide-scavenging activity of polyhydroxylated fullerenol, C60(OH)24. Nitric Oxide. 2004;11:201–207.

(18) Matsushima T, Hayashi M, Matsuoka A, Ishidate M Jr, Miura KF, Shimizu Y, et al. Validation study of the in vitro micronucleus test in a Chinese hamster lung cell line (CHL/IU). Mutagenesis. 1999;14:569–580.

(19) Kamat JP, Devasagayam TP, Priyadarsini KI, Mohan H. Reactive oxygen species mediated membrane damage induced by fullerene derivatives and its possible biological implications. Toxicology. 2000;155:55–61.

(20) Antoccia A, Tanzarella C, Modesti D, Degrassi F. Cytokinesis-

block micronucleus assay with kinetochore detection in colchicine-treated human fibroblasts. Mutat Res. 1993;287: 93–99.

(21) Cimini D, Tanzarella C, Degrassi F. Differences in malsegregation rates obtained by scoring ana-telophases or binucleate cells. Mutagenesis. 1999;14:563–568.

(22) Kirsch-Volders M, Elhajouji A, Cundari E, Van Hummelen P. The in vitro micronucleus test: a multi-endpoint assay to detect simultaneously mitotic delay, apoptosis, chromosome breakage, chromosome loss and non-disjunction. Mutat Res. 1997;392:19–30.

(23) Yamago S, Tokuyama H, Nakamura E, Kikuchi K, Kananishi S, Sueki K, et al. In vivo biological behavior of a water-miscible fullerene: 14C labeling, absorption, distribution, excretion and acute toxicity. Chem Biol. 1995;2:385–389.

Circ J 2007; **71:** 437–444

Nanomaterials Induce Oxidized Low-Density Lipoprotein Cellular Uptake in Macrophages and Platelet Aggregation

Yasuharu Niwa, PhD; Naoharu Iwai, MD

Background Nanomaterials have numerous potential benefits for society, but the potential hazards of nanomaterials on human health are poorly understood. Nanomaterials are known to pass into the circulatory system in humans, causing vascular injuries that might play a role in the development of atherosclerosis. The present study aimed to determine the effects of chronic exposure to nanomaterials on macrophage phenotype and platelet aggregation.

Methods and Results Cultured macrophages (RAW264.7) were treated with carbon black (CB) and water-soluble fullerene ($C_{60}(OH)_{24}$) from 7 to 50 days. Individually, CB had no significant effects on RAW264.7 cell growth, whereas $C_{60}(OH)_{24}$ alone or CB and $C_{60}(OH)_{24}$ together with oxidized low-density lipoprotein (Ox-LDL) (100 μg/ml) induced cytotoxic morphological changes, such as Ox-LDL uptake-induced foam cell-like formation and decreased cell growth, in a dose-dependent manner. $C_{60}(OH)_{24}$ induced LOX-1 protein expression, pro-matrix metalloprotease-9 protein secretion, and tissue factor mRNA expression in lipid-laden macrophages. Although CB or $C_{60}(OH)_{24}$ alone did not induce platelet aggregation, $C_{60}(OH)_{24}$ facilitated adenosine diphosphate (ADP)-induced platelet aggregation. Furthermore, $C_{60}(OH)_{24}$ acted as a competitive inhibitor of ADP receptor antagonists in ADP-mediated platelet aggregation.

Conclusions The present study confirmed novel effects of nanomaterials in macrophages and platelets. These effects suggest that exposure to nanomaterials might be a risk for atherothrombotic diseases. (*Circ J* 2007; **71:** 437–444)

Key Words: Atherosclerosis; Lipid-laden macrophages; Nanomaterials; Platelet aggregation

The advent of nanomaterials has provided incredible opportunities for biomedical applications such as therapeutic and diagnostic tools, in addition to applications in engineering, electronics and optics[1–3] Biomedical applications under development include targeted drug delivery systems for the brain and tumor tissues and intravascular nanosensor and nanorobotic devices for imaging and diagnosis. However, the potential adverse effects of nanomaterials on human health remains to be established[4–6]

Potential exposure pathways for nanomaterials have been proposed in humans[5,7] Although inhalation might be a major route of exposure, ingestion and dermal exposure are also possible during the nanomaterial manufacture. After inhalation, nanomaterials are deposited in the respiratory tract, and their small size allows cellular uptake and transcytosis into the blood and lymphatic system. Our experiments have shown that both carbon black (CB) and water-soluble fullerene ($C_{60}(OH)_{24}$) exhibit cytotoxicity in human umbilical vein endothelial cells (HUVEC), such as decreased cell density and cell growth. Furthermore, CB and $C_{60}(OH)_{24}$ upregulated the expression of inflammation-related genes and ubiquitin-proteasome-related genes in HUVEC. These results suggest that exposure to CB and/or $C_{60}(OH)_{24}$ might be a risk for atherothrombotic diseases[8,9]

(Received June 13, 2006; revised manuscript received December 6, 2006; accepted December 19, 2006)

Department of Epidemiology, Research Institute, National Cardiovascular Center, Suita, Japan

Mailing address: Yasuharu Niwa, PhD, Department of Epidemiology, Research Institute, National Cardiovascular Center, Suita 565-8565, Japan. E-mail: yniwa@ri.ncvc.go.jp

In addition to endothelium, macrophages and platelets are important players for atherogenesis. Macrophages under the endothelium may take up denatured-low-density lipoprotein (LDL) (oxidized-LDL; Ox-LDL and acetylated-LDL; Ac-LDL) and become foam cells. The lipid-laden macrophages play a key role in inducing plaque rupture by secreting proteases, such as a matrix metalloprotease-9 (MMP-9) that destroys the extracellular matrix. Finally, rupture of advanced atherosclerotic plaques can lead to platelet aggregation, which results in atherothrombotic events.

In the present study, we aimed to clarify the effects of chronic exposure of nanomaterials, such as CB and $C_{60}(OH)_{24}$, on macrophages phenotypes and the aggregating effects of CB and $C_{60}(OH)_{24}$ on platelets.

Methods

Materials

CB (Association of Powder Process Industry and Engineering, Japan) and $C_{60}(OH)_{24}$ (Tokyo Progress Sysytem, Tokyo, Japan) were prepared as described previously[9] Fluoresbrite carboxylate microspheres (diameter, 6 μm) were obtained from Polysciences Inc (PA, USA).

Cell Culture

Mouse macrophages cell lines (RAW264.7) were obtained from Dainippon Sumitomo Phrma (Osaka, Japan) and were cultured in RPMI1640 with 10% (v/v) fetal bovine serum (Hyclone, Utah, USA). Cells were cultured in RPMI1640 with 2% (v/v) fetal bovine serum plus sonicated CB (0–100 μg/ml) or $C_{60}(OH)_{24}$. Cells were passaged every 3–4 days.

Lactate Dehydrogenase (LDH) Assay

LDH activity was analyzed with a CytoTox 96 non-radioactive cytotoxicity assay kit (Promega, Madison, USA) according to the manufacturer's protocols. RAW264.7 cells at 50–60% confluence were treated with CB or $C_{60}(OH)_{24}$ alone for 24 h, or 13 or 50 days. In addition, cells at 50–60% confluence were treated with CB or $C_{60}(OH)_{24}$ for 50 days or 8 days, respectively, and Ox-LDL was then added (Biomedical Technologies, MA, USA) (0–100 μg/ml) for a further 2 days. LDH activity in the culture medium was measured based on absorbance at 490 nm using a microplate reader (ARVO; PerkinElmer, Japan). Cytotoxicity was expressed relative to basal LDH release in untreated controls. Cells at 50–60% confluence were treated with $C_{60}(OH)_{24}$ for 8 days or 6-μm beads for 3 days, and Ox-LDL or Dil-Ac-LDL (Biomedical Technologies) was then added for 24 h. Cells were examined under a microscope (Zeiss Axiovert 25, Göttingen, Germany).

Proliferation Assay

Cell proliferation assay was carried out using a Cell Counting-8 kit (Dojindo Laboratories, Kumamoto, Japan) according to the manufacturer's protocols. Cells were cultured in 12-well plates, and were treated with Ox-LDL (100 μg/ml) for 5 days to induce foam cell-like formation, after which $C_{60}(OH)_{24}$ (0–100 ng/ml) was added to the cells for a further 2 days. Cell growth was measured based on absorbance at 450 nm as detected by the ARVO micro-plate reader.

Treated and untreated cells were fixed with 4% paraformaldehyde for 15 min at room temperature. After washing, cells were stained with filtered Oil Red O solution (60% isopropanol) or Giemsa solution for 0.5 h–2 h at room temperature. After washing, the cells were examined under a microscope (Olympus BX-51, Tokyo, Japan). The Dil-Ac-LDL incorporated macrophages were captured directly from an RGB camera attached to the microscope (Zeiss Axiovert 25, Göttingen, Germany) and displayed on a Adobe photoshop CS2 to quantify fluoro-intensity in macrophages.

Western Blotting of LOX-1 and SR-AI

Samples were obtained from RAW264.7 cells treated with lysis buffer (20 mmol/L Tris-HCl, pH 7.4, with 150 mmol/L NaCl, 1 mmol/L EDTA, 1 mmol/L EGTA, 2.5 mmol/L sodium pyrophosphate, 1 mmol/L β-glycerol phosphate, 1 mmol/L Na_3VO_4, 1 μg/ml leupeptin, 0.1% protease inhibitor cocktail (Nacarai Tesque, Kyoto, Japan), and 1% Triton X-100). Equal amounts of proteins (10 μg/ml) were subjected to reducing sodium dodecylsulfate–polyacrlamide gel (10%) electrophoresis electrophoresis after boiling with 1 mmol/L dithiothreithol and were transferred to nitrocellulose membranes. (Pall Corporation, Ann Arbor, MI, USA). After blocking with 5% (w/v) skim-milk in T-TBS (10 mmol/L Tris-HCl, pH 7.5 with 10 mmol/L sodium chloride and 0.1% Tween 20) buffer, the membrane was incubated with primary antibody (R&D biosystems, MN, USA) (LOX-1; 1:100 dilution, scavenger receptor-type AI (SR-AI); 2 μg/ml) at 4°C overnight. After washing, the membrane was incubated with secondary antibody (anti-mouse horseradish peroxidase-conjugated antibody and anti-rat horseradish peroxidase-conjugated antibody, respectively; 1:5,000-10,000 dilution) at room temperature for 1 h. LOX-1, SR-AI and β-actin protein were visualized using the ECL system (Amersham Biosciences, Buckinghamshire, UK).

Pro-MMP-9 Secretion Assay

Culture medium was collected from cells treated with $C_{60}(OH)_{24}$ alone for 10 days or with $C_{60}(OH)_{24}$ for 8 days followed by 2 days of co-treatment with Ox-LDL (100 μg/ml). Pro-MMP-9 in culture medium was analyzed using a mouse pro-MMP-9 sandwich enzyme-linked immunosorbent assay kit (B&D systems, MN, USA) according to the manufacturer's protocols. Pro-MMP-9 in culture medium was detected by absorbance at 450 nm, and concentration was calculated using a standard curve.

Reverse Transcription (RT)-Polymerase Chain Reaction (PCR) for Tissue Factor mRNA Expression

Expression of tissue factor mRNA in cells treated with $C_{60}(OH)_{24}$ alone for 10 days or with $C_{60}(OH)_{24}$ for 8 days followed by 2 days with Ox-LDL (100 μg/ml) and were quantified by RT-PCR. Tissue factor primer sets were as follows: tissue factor; forward 5'-CGGGTGCAGGCATT CCAGAG-3' and reverse 5'-CTCCGTGGGACAGAGAG-GAC-3', glucose-3-phosphate dehydrogenase; forward 5'-ACCACAGTCCATGCCATCA-3' and reverse 5'-TCCAC CACCCTGTTGCTGTA-3'. The PCR products were electrophoresed on 2% agarose gels, and were stained with ethidium bromide, visualized using ultraviolet and recorded. Expression levels of tissue factor were adjusted against glucose-3-phosphate dehydrogenase expression levels.

Platelet Aggregation Assay

Whole blood was collected from the ear artery of male Japanese white rabbits (n=3; body weight, 3–5 kg) into tubes containing 3.8% (w/v) tri-sodium citrate, and were kept at room temperature for 5–10 min. After pre-treatment with or without CB (5 μg/ml) or $C_{60}(OH)_{24}$ (5 μg/ml) at room temperature for 5 min, ticlopydine hydrochloride (0–4 mmol/L) was added to whole blood, which was then left to stand at room temperature for a further 15 min. Adenosine diphosphate (ADP) (0–80 mmol/L) induced aggregation was analyzed using a whole blood filtration pressure aggregometer (WBA analyzer, Yokohama, Japan)![10] Reaction tubes containing 200 μl aliquots of whole blood were placed an incubation chamber at 37°C for 2 min, followed by addition of 22.2 μl of ADP. The pressure rate was standardized using a grading curve of 4 different ADP concentrations (0, 1, 2, 4, 8 mmol/L or 0, 10, 20, 40, 80 mmol/L, respectively) on the x-axis and pressure rate on the y-axis. The concentration of ADP causing an increase in pressure rate was calculated and was applied as the platelet aggregatory threshold index. Experiments were performed at least 3 times.

Statistical Analysis

Data are shown as means ± SD. Statistical evaluation was performed by ANOVA. Values of $p<0.05$ were considered statistically significant.

Results

Effects of CB on RAW264.7

The effects of chronic exposure to CB were examined by treating RAW264.7 cells with CB (0–100 μg/ml) for 24 h, 13 days and 50 days. We observed marked CB (100 μg/ml) uptake in RAW264.7 cells at days 13 and 50 (Figs 1B, d and C, d). However, cytotoxic morphological changes, such as cytosolic phagosome formation, cell disorientation and decreased cell density, were not observed (Figs 1A, B and C, a–d). No significant cytotoxic injury (based on LDH

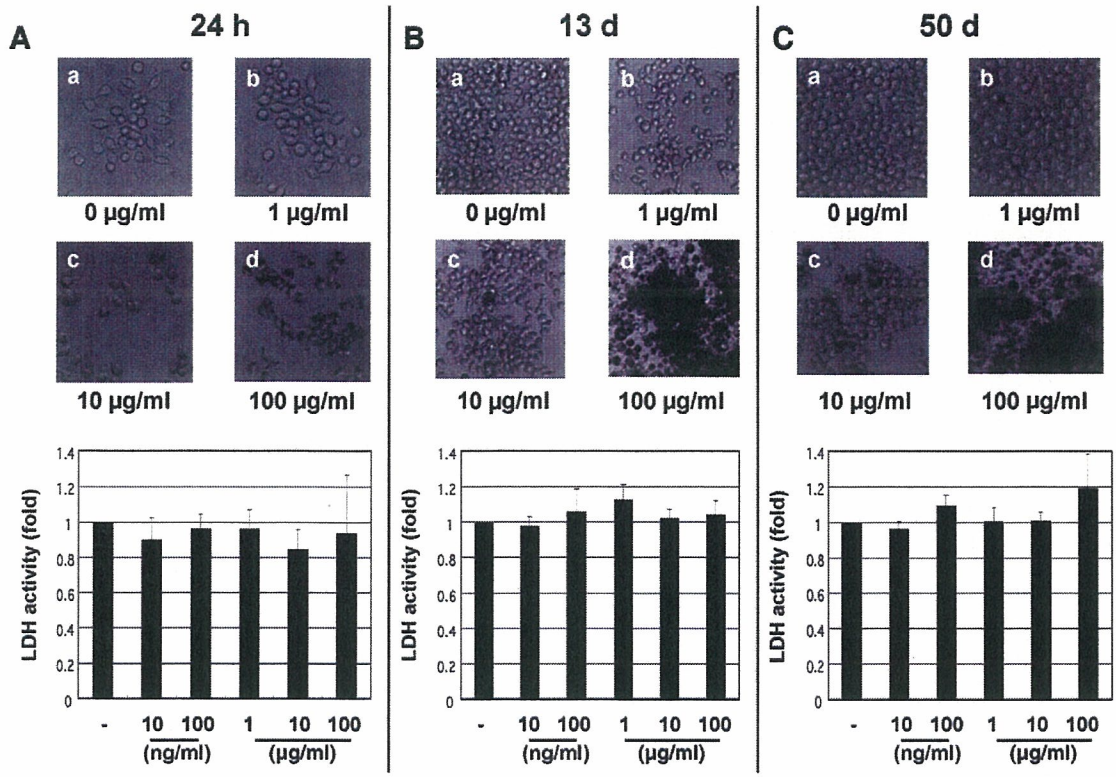

Fig 1. Representative photomicrographs of RAW264.7 cells treated with carbon black (CB). (A) RAW264.7 cells were treated with CB (a, 0 μg/ml; b, 1 μg/ml; c, 10 μg/ml; d, 100 μg/ml) for 24 h, (B) 13 days or (C) 50 days, upper panel (×200 magnification). CB did not induce cytotoxic injury in RAW264.7 cells. RAW264.7 cells were cultured with CB (0, 10 ng/ml, 100 ng/ml, 1 μg/ml, 10 μg/ml or 100 μg/ml) for (A) 24 h, (B) 13 days or (C) 50 days. Culture medium was then collected. Lactate dehydrogenase (LDH) released into supernatant was measured relative to basal LDH release in controls (control ratio = 1.0) (n=4), lower panel.

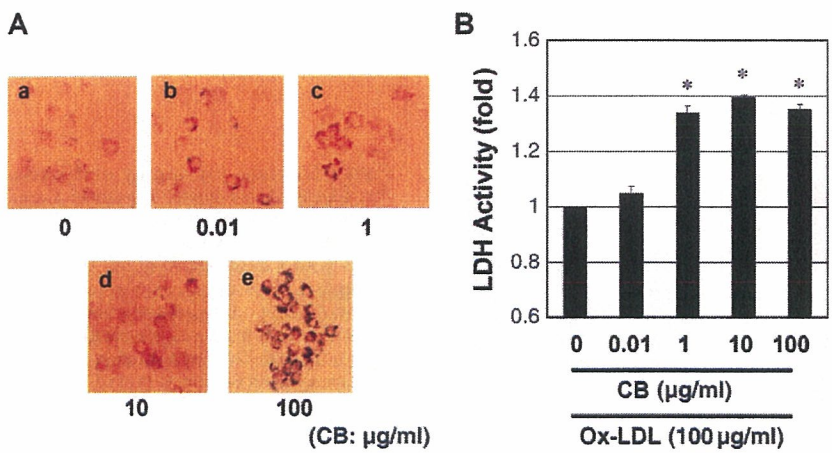

Fig 2. Oxidized low-density lipoprotein (Ox-LDL)-induced cytotoxic injury in carbon black (CB)-treated RAW264.7 cells. (A) After RAW264.7 cells were cultured with CB (a, 0 ng/ml; b, 10 ng/ml; c, 1 μg/ml; d, 10 μg/ml; e, 100 μg/ml) for 48 days, and were then co-treated with Ox-LDL (100 μg/ml) for a further 48 h. Cells were fixed with 4% paraformaldehyde neutralized buffered solution, and were then stained with Oil Red O (a–d). (B) RAW264.7 cells were cultured with CB (0, 10 ng/ml, 100 ng/ml, 1 μg/ml, 10 μg/ml or 100 μg/ml) for 48 days, and were then co-treated with Ox-LDL (100 μg/ml) for a further 48 h. Culture medium was collected, and lactate dehydrogenase (LDH) was measured relative to basal LDH release in controls (CB and Ox-LDL=0 μg/ml) (control ratio = 1.0). *$p<0.05$ vs controls.

activity) was seen in RAW264.7 cells at any time point (24 h, 13 days and 50 days) (Figs 1A–C).

CB Together With Ox-LDL Induces Injury in RAW264.7

To determine the effects of Ox-LDL (100 μg/ml) on chronic exposure to CB (0–100 μg/ml) in RAW264.7 cells, we performed Oil Red O staining. Cells were cultured in CB-containing medium for 48 days and were then treated with Ox-LDL for 2 days. Dose-dependent Oil Red O staining was seen with CB treatment (Fig 2A). LDH activity after Ox-LDL treatment was also dependent on CB concentration (peak LDH activity was observed at 10 μg/ml CB) (Fig 2B). These data suggest that CB itself may not be cytotoxic to RAW264.7 cells, but when cells are co-treated with CB and Ox-LDL, LDH secretion was elevated in a CB dose-dependent manner, and Ox-LDL uptake was also increased.

$C_{60}(OH)_{24}$ Induces Cytotoxic Morphological Changes in RAW264.7

RAW264.7 cells were treated with $C_{60}(OH)_{24}$ for 24 h to 10 days. $C_{60}(OH)_{24}$ (20 ng/ml), which is the predicted natu-

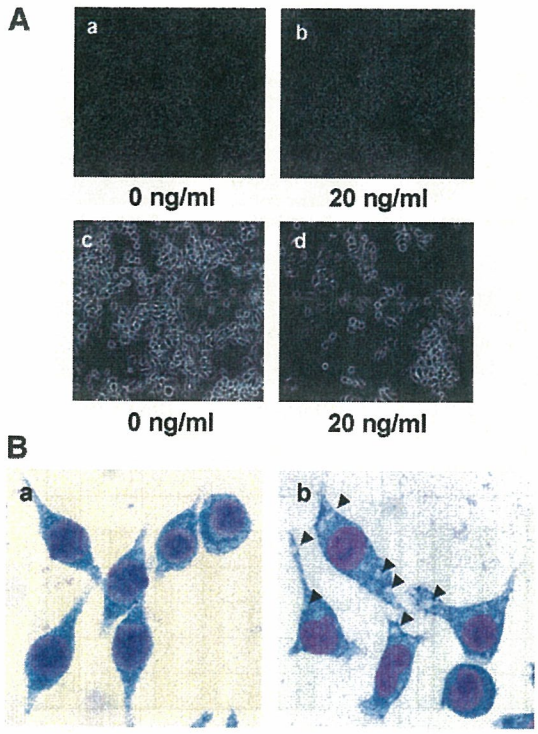

Fig 3. Water-soluble fullerene ($C_{60}(OH)_{24}$) induced phagosome formation in RAW264.7 cells. (A) Cells were treated with $C_{60}(OH)_{24}$ (a, 0 ng/ml; b, 20 ng/ml) for 24 h or 10 days (c, 0 ng/ml; d, 20 ng/ml), and cell morphology was then visualized (×200 magnification). (B) Cells were treated with $C_{60}(OH)_{24}$ (0, 20 ng/ml) for 10 days, and the cells were then fixed with 4% (v/v) paraformaldehyde neutralized buffered solution, and stained with Giemsa. Cells were then examined by microscope (×1,000 magnification). Arrowheads indicate phagosomes.

ral environmental concentration,[11] induced cytotoxic morphological changes in RAW264.7, including phagosome-like formation in the cytosol and decreased cell density (Fig 3A). Phagosome formation was confirmed by Giemsa staining (Fig 3B, arrowheads).

$C_{60}(OH)_{24}$ Together With Ox-LDL Induces Injury in RAW264.7

To determine the effects of Ox-LDL (100 μg/ml) on $C_{60}(OH)_{24}$ (0–100 ng/ml)-induced cell injury, we performed Oil Red O staining. Cells were cultured with $C_{60}(OH)_{24}$ for 8 days, and were then co-treated with Ox-LDL for 2 days. Enhanced Oil Red O staining was seen in a dose-dependent manner with $C_{60}(OH)_{24}$ and Ox-LDL co-treatment (Figs 4A, d–f), but Oil Red O staining cells was not seen when treated with $C_{60}(OH)_{24}$ alone (Figs 4A, a–c). Increases in LDH activity were dependent on $C_{60}(OH)_{24}$ concentration (LDH maximum activity was observed at 100 ng/ml $C_{60}(OH)_{24}$) in the presence of Ox-LDL (Fig 4B). RAW264.7 cells were also treated with Ox-LDL (100 μg/ml) for 5 days followed by $C_{60}(OH)_{24}$ (20, 100 ng/ml) for a further 48 h. Cells were stained by Oil Red O in a $C_{60}(OH)_{24}$ dose-dependent manner (Fig 4C). In addition, cell growth was dose-dependenly suppressed by $C_{60}(OH)_{24}$ in the pre-treatment with Ox-LDL (Fig 4D). CB alone had no cytotoxic effects, however, $C_{60}(OH)_{24}$ alone had significant cytotoxicities appreared in macrophages. We focused on the characterization of $C_{60}(OH)_{24}$ cytotoxicities in further experiments.

$C_{60}(OH)_{24}$ Induces LOX-1 Expression in RAW264.7

CB and $C_{60}(OH)_{24}$ induced endocytotic uptake of Ox-LDL in RAW264.7 cells, which were strongly stained with Oil Red O. This indicates that expression of Ox-LDL receptors, such as LOX-1, is elevated in RAW264.7 cells. To identify LOX-1 protein expression in RAW264.7, we performed immunoblotting using whole cell extracts. LOX-1 expression was induced by $C_{60}(OH)_{24}$ in a dose-dependent

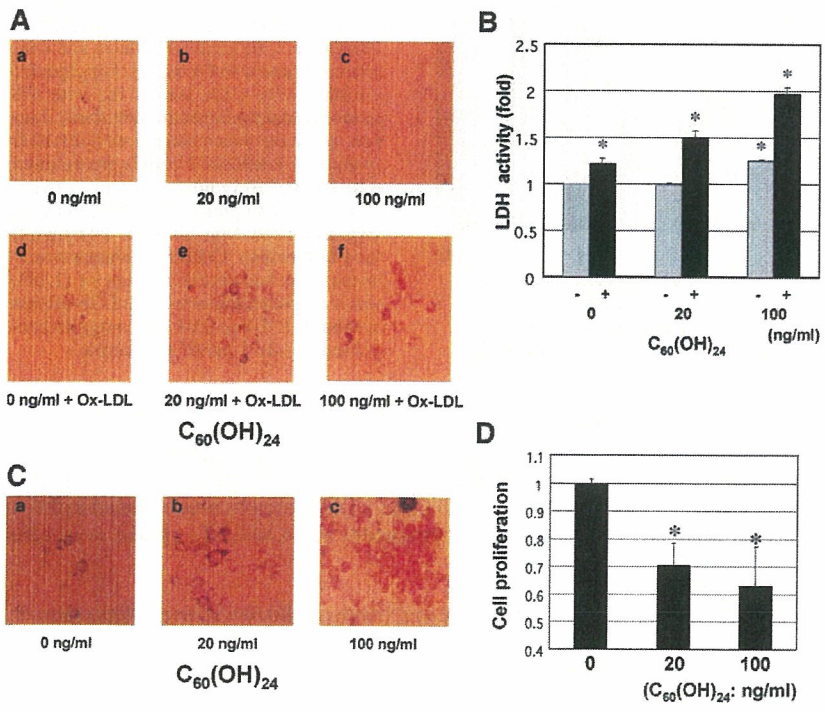

Fig 4. Oxidized low-density lipoprotein (Ox-LDL)-induced cytotoxic injury in water-soluble fullerene ($C_{60}(OH)_{24}$)-treated RAW 264.7 cells. (A) RAW264.7 cells were cultured with $C_{60}(OH)_{24}$ (0 ng/ml, 20 ng/ml, 100 ng/ml) for 8 days and were co-treated with Ox-LDL (100 μg/ml) for a further 48 h. Cells were then fixed with 4% paraformaldehyde neutralized buffered solution and were then stained with Oil Red O (a–f). Cells were visualized by microscopy (×400 magnification). (B) Cells were cultured with $C_{60}(OH)_{24}$ (0, 20 or 100 ng/ml) for 8 days, and were then co-cultured with (+) or without (–) Ox-LDL (100 μg/ml) for a further 48 h. Culture medium was collected and lactate dehydrogenase (LDH) activity was measured. *$p<0.05$ vs controls. (C) RAW264.7 cells were cultured with Ox-LDL (100 μg/ml) for 5 days, and were then co-cultured with $C_{60}(OH)_{24}$ (a, 0 ng/ml; b, 20 ng/ml; c, 100 ng/ml) for a further 48 h. Cells were then fixed and stained with Oil Red O. (D) Cell growth was inhibited by co-treatment with $C_{60}(OH)_{24}$ and Ox-LDL. Cell growth was analyzed using cell counting kit-8. Results are relative to controls (n=4). *$p<0.05$ vs controls.

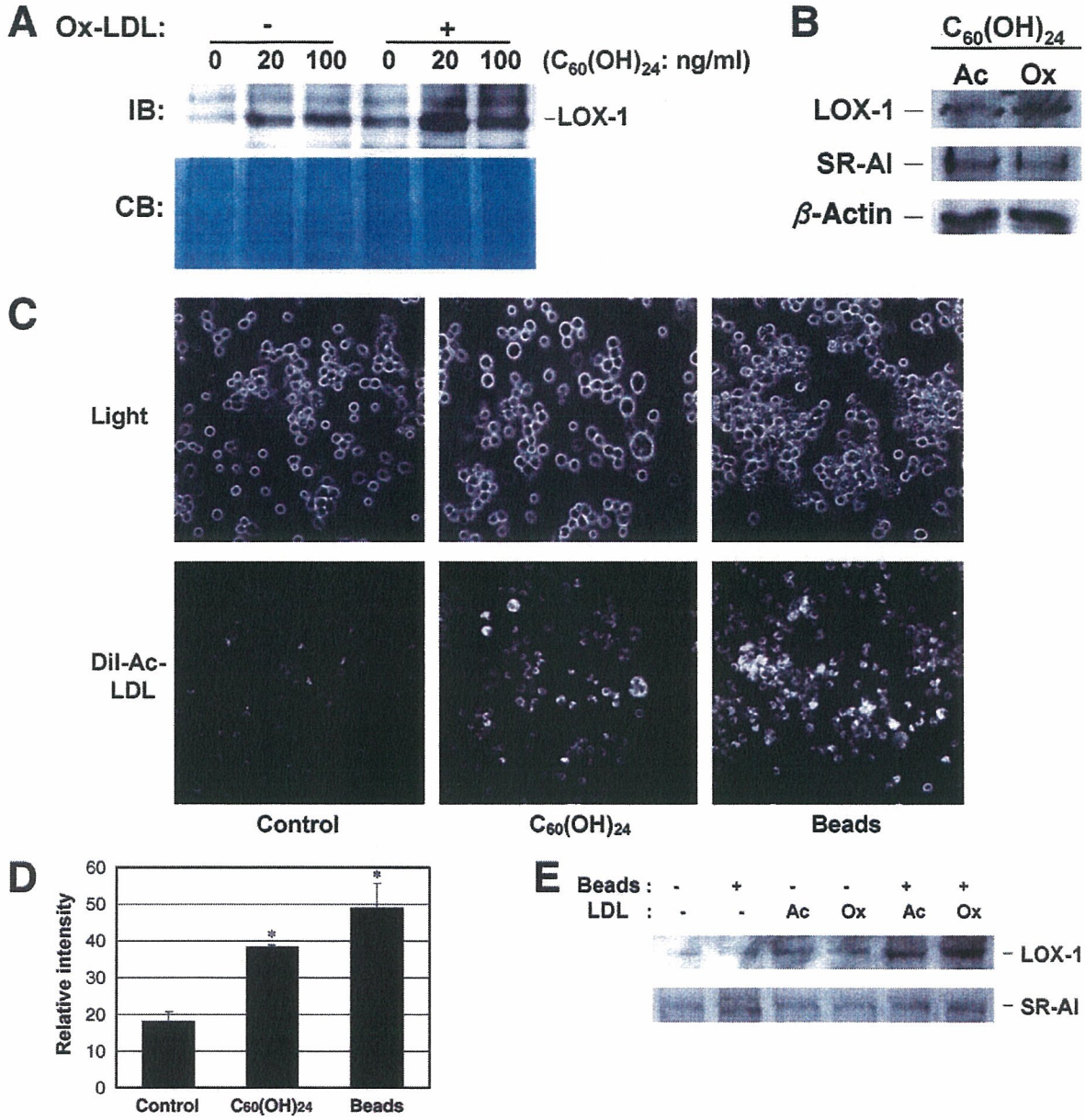

Fig 5. Water-soluble fullerene ($C_{60}(OH)_{24}$) and 6-μm bead-induced LOX-1 expression in RAW264.7 cells. Cells were cultured with $C_{60}(OH)_{24}$ (0, 20 or 100 ng/ml) for 8 days, co-cultured with (+) or without (–) oxidized low-density lipoprotein (Ox-LDL) (100 μg/ml) for a further 48 h and harvested. Whole cell extracts were prepared for sodium dodecylsulfate–polyacrlamide gel electrophoresis (SDS–PAGE). Samples (10 μg/ml) were loaded on reducing SDS–PAGE gels (10%) electrophoresis, and were transferred to membranes for immunoblotting (IB) (LOX-1 1:100, scavenger receptor-type AI (SR-AI): 2 μg/ml). LOX-1 protein or SR-AI protein expression was visualized by enzymatic chemiluminescence (ECL). Equal amounts of protein for Western blotting were confirmed by Coomassie blue staining or β-actin as control (A, B). Dil-acetylated-low-density lipoprotein (Dil-Ac-LDL) incorporation was investigated by pre-treatment with $C_{60}(OH)_{24}$ for 8 days or 6-μm beads for 3 days (beads), or no pre-treatment (control), after which Dil-Ac-LDL (5 μg/ml) was added to RAW264.7 cells. Cells were examined by fluoro-microscopy (×200 magnification) (C). The Dil-Ac-LDL (5 μg/ml) incorporated macrophages were captured directly from RGB camera attached to the microscope and displayed on Adobe photoshop CS2 to quantify of fluoro-intensity in macrophages. $p<0.03$ vs controls (D) Cells were treated with 6-μm beads for 3 days. Ox-LDL or acetylated-LDL was added for 24 h, and cells were harvested. Whole-cell extracts were prepared for SDS–PAGE. Samples (30 μg/ml) were loaded on reducing gels (10%), and were then transferred to membranes for IB (LOX-1 1:100, SR-AI: 2 μg/ml). Protein expression was visualized by ECL (E). CB, carbon black.

manner, and was further stimulated in the presence of Ox-LDL (Fig 5A). In contrast, SR-AI expression was not significantly induced by co-treatment with $C_{60}(OH)_{24}$ and Ox-LDL or Ac-LDL in RAW264.7 cells (Fig 5B). In addition, 6-μm fluoro beads induced endocytotic uptake of Ac-LDL in RAW264.7 cells (Fig 5D). LOX-1 expression was not induced by 6-μm beads, but was stimulated by co-treatment with Ox-LDL or Ac-LDL (Figs 5C,E). LOX-1 protein expression was more strongly stimulated by Ox-LDL than Ac-LDL (Figs 5B,E).

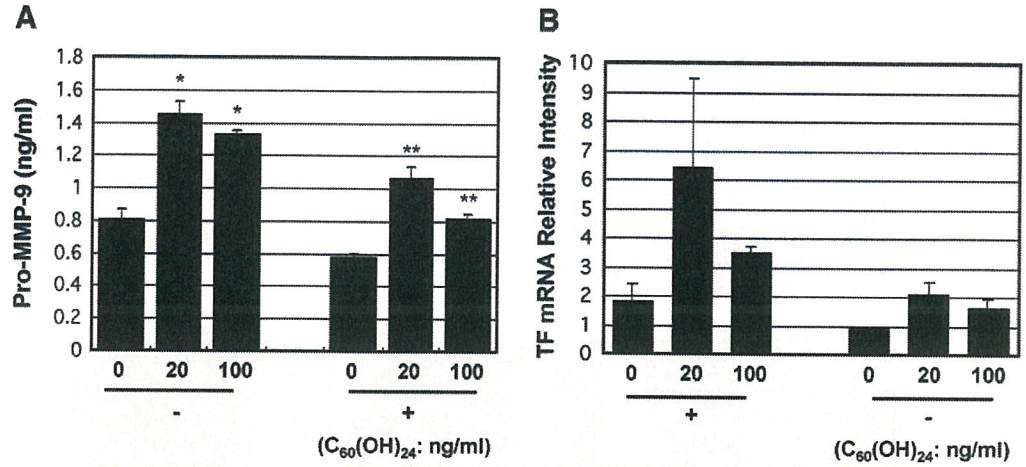

Fig 6. Water-soluble fullerene ($C_{60}(OH)_{24}$)-induced pro-matrix metalloprotease-9 (MMP-9) secretion and tissue factor (TF) mRNA expression. Cells were cultured with $C_{60}(OH)_{24}$ (0, 20 or 100 ng/ml) for 8 days and were then co-cultured with (+) or without (–) oxidized low-density lipoprotein (Ox-LDL) (100 μg/ml) for a further 48 h, after which culture medium was collected for pro-MMP-9 enzyme-linked immunosorbent assay (n=4) (A), and total RNA was extracted from the cells for TF reverse transcription-polymerase chain reaction experiments (n=3) (B). *$p<0.02$ vs controls (0 ng/ml), **$p<0.05$ vs controls (0 ng/ml).

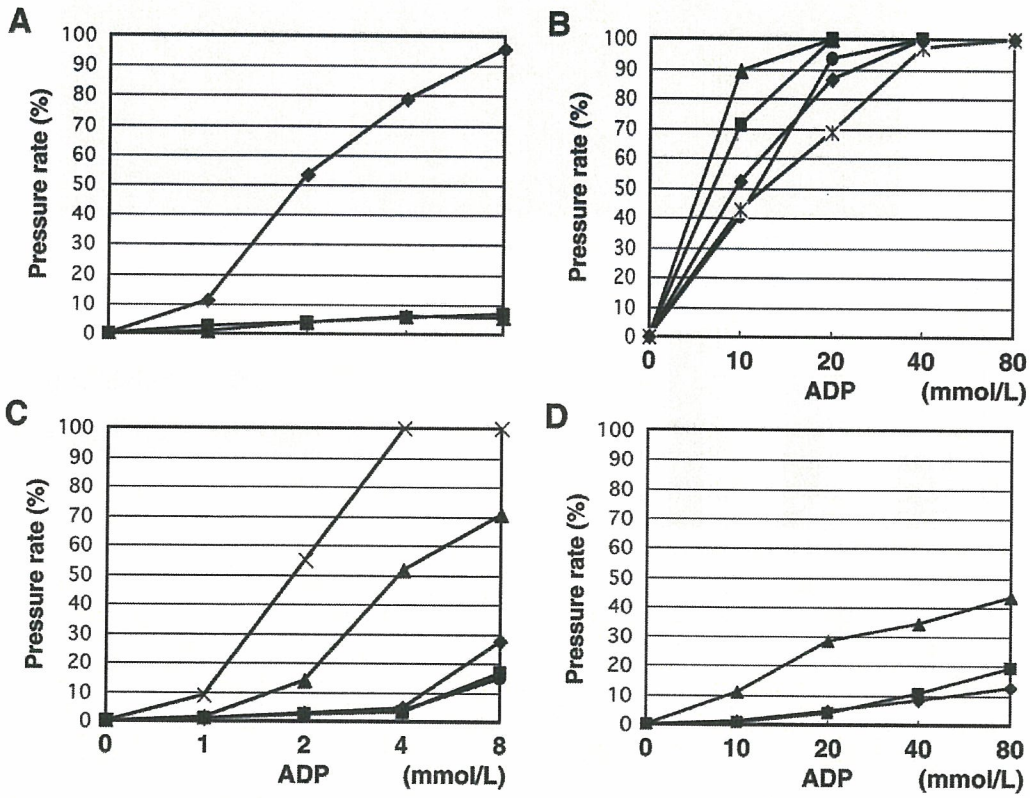

Fig 7. Platelet aggregation, as analyzed by screen filtration pressure method in carbon black (CB) or water-soluble fullerene ($C_{60}(OH)_{24}$)-treated whole blood. (A) Concentration response curve of platelet aggregation to adenosine diphosphate (ADP) (◆: 0, 10, 20, 40, 80 mmol/L), CB (▲; 0, 50, 100, 200 μg/ml) and $C_{60}(OH)_{24}$ (■; 0, 5, 10, 25, 50 μg/ml). (B) High-concentration ADP (●; 0, 10, 20, 40, 80 mmol/L), CB (*; 50 μg/ml, ◆; 100 μg/ml), $C_{60}(OH)_{24}$ (■; 25 μg/ml, ▲; 50 μg/ml), and (C) low-concentration ADP (◆; 0, 1, 2, 4, 8 mmol/L). ADP-induced aggregation was facilitated by $C_{60}(OH)_{24}$ (■; 2.5 μg/ml, ▲: 25 μg/ml, ×; 50 μg/ml) in a dose-dependent manner, but CB (*; 50 μg/ml, ●; 100 μg/ml) had no effect. (D) High-concentration ADP (0, 10, 20, 40, 80 mmol/L), $C_{60}(OH)_{24}$ (■; 2.5 μg/ml, ▲; 10 μg/ml) upregulated platelet aggregation, despite inhibition by ticlopidine hydrochloride (◆; 2 mmol/L).

$C_{60}(OH)_{24}$ Induces Pro-MMP-9 Secretion and Tissue Factor mRNA Expression in RAW264.7

To assess whether pro-MMP-9 may be secreted from in RAW264.7 cells, cells were treated with $C_{60}(OH)_{24}$ (0–100 ng/ml) for 8 days and Ox-LDL (100 μg/ml) was added for 2 further days of culture. Sandwich ELISA against for pro-MMP-9 was then performed. The amounts of pro-MMP-9 secreted into culture medium were significantly increased in the presence of $C_{60}(OH)_{24}$, and under co-treatment conditions with Ox-LDL and $C_{60}(OH)_{24}$, although the amount of secreted pro-MMP-9 was 25% lower under the co-treatment conditions (Fig 6A). Tissue factor mRNA expression was approximately 2-fold higher with $C_{60}(OH)_{24}$, and was approximately 6-fold higher after $C_{60}(OH)_{24}$ stimulation (Fig 6B). These results show that $C_{60}(OH)_{24}$ alone facilitates pro-MMP-9 secretion and tissue factor mRNA expression via an unknown pathway in RAW264.7 cells.

$C_{60}(OH)_{24}$ and CB Effects on Platelet Aggregation

The effects of CB or $C_{60}(OH)_{24}$ on platelet function were examined by evaluating ADP-induced whole blood aggregation using the filtration pressure method. $C_{60}(OH)_{24}$ does not stimulate platelet aggregation in vitro[12] We also found that CB and $C_{60}(OH)_{24}$ alone do not induce platelet aggregation (Fig 7A). However, we hypothesized that CB or $C_{60}(OH)_{24}$ might affect ADP-dependent platelet aggregation. When whole blood was pretreated with $C_{60}(OH)_{24}$, ADP-induced aggregation threshold index values were elevated in a dose-dependent manner (Figs 7B,C). Thus, $C_{60}(OH)_{24}$ facilitates ADP-induced aggregation, and this function was dependent on the ADP receptor (Fig 7D), as collagen- and thrombin-induced platelet aggregation threshold index values did not significantly change when whole blood was pre-treated with CB or $C_{60}(OH)_{24}$ (data not shown). These results show that $C_{60}(OH)_{24}$ specifically facilitates ADP-induced platelet aggregation.

Discussion

Epidemiologic and animal studies have suggested that exposure to nanoparticles plays a role in cardiovascular diseases such as atherosclerosis and myocardial infarction[13–20] For example, traffic-derived nanoparticles are suspected to be a risk for cardiovascular diseases[21]

Our studies have recently shown that CB and $C_{60}(OH)_{24}$ exert cytotoxic effects on HUVEC, presumably via phagocytotic cell death dependent on further ubiquitination of cytosolic proteins[9] Endothelial cell injury, inflammation, and impairment of membrane integrity are closely related to the initiation of atherosclerosis and ischemic heart disease[22,23] Nanomaterial cytotoxicity in cells varies with chemical characteristics and surface properties of the molecule, including hydrophobicity, hydrophilicity and surface area per molecule[4,18] The purpose of the current study was to clarify the effects of chronic exposure to low-dose nanomaterials, such as CB or $C_{60}(OH)_{24}$, particularly with regard to the cardiovascular system in vitro and in vivo. The present study indicates that CB alone has no significant cytotoxic actions in macrophages; however, cytotoxicity was markedly enhanced by co-treatment with Ox-LDL. In contrast, $C_{60}(OH)_{24}$ alone has significant cytotoxic actions and cytotoxicity was markedly enhanced by co-treatment with Ox-LDL (Figs 2B,4B).

We analyzed the phagocytotic functions of RAW264.7 cells toward Ox-LDL or Ac-LDL after pre-treatment with 6-μm fluoro beads or 20 ng/ml $C_{60}(OH)_{24}$ in cells. Treatment with 6-μm fluoro beads stimulated Ac-LDL incorporation to a greater degree than pre-treatment with $C_{60}(OH)_{24}$ in RAW264.7 cells (Fig 5D). We proposed that microparticles, as well as nanoparticles, are able to stimulate phagocytotic system: however, microparticles more strongly stimulated the phagocytotic function of RAW264.7 cells. Further stimulated phagocytotic function caused cell death in RAW264.7 cells treated with 6-μm fluoro beads for 4 days (data not shown). Interestingly, $C_{60}(OH)_{24}$ alone might induce LOX-1 protein expression; $C_{60}(OH)_{24}$ activated stress-related kinases, such as p38 MAPK, thus contribute to phagosome maturation in macrophages[24,25] and leading to activation of nuclear factor (NF)-κB, which is a major transcriptional factor for LOX-1[26] LOX-1 gene expression is dynamically modulated by tumor necrosis factor-α, transform growth factor-β, angiotensin II, endothelin-1 and peroxisome proliferator-activated receptor-a via NF-κB activation[27–29] and stimulate cell injury or suppress cell growth. Nanomaterials might affect the activity of Ox-LDL receptors, such as CD36, SR-A and LOX-1, on the macrophage plasma membrane, thus triggering the process of phagocytosis and Ox-LDL uptake. We also found that $C_{60}(OH)_{24}$ induced secretion of pro-MMP-9. Macrophage-mediated proteolysis participates in the rupture of atherosclerotic plaques and MMP-9 might be involved in this process. Recent studies have indicated that the proteolytic activity of MMP-9 is sufficient to induce the rupture of advanced atherosclerotic lesions in apoE-/- mice[30,31] These results suggest that nanomaterials might contribute to the rupture of advanced atherosclerosis by stimulating MMP-9 secretion from macrophage-derived foam cells.

CB and $C_{60}(OH)_{24}$ did not directly cause activation and aggregation of platelets in vitro. This observation was also reported by Radomski et al in experiments on nanomaterials and platelet aggregation[12] Although $C_{60}(OH)_{24}$ alone did not activate platelet aggregation, when platelets were pre-treated with $C_{60}(OH)_{24}$, ADP-induced aggregation was 10–20% higher and this increase was $C_{60}(OH)_{24}$ dose-dependent (Figs 7B,C). Furthermore, ADP-induced platelet aggregation was inhibited by more than 80% by ticlopidine hydrochloride (2–4 mmol/L), an ADP receptor (P2Y12) antagonist[32] but after platelets were pre-treated with $C_{60}(OH)_{24}$, inhibition by ticlopidine hydrochloride (2 mmol/L) was suppressed. This indicates that $C_{60}(OH)_{24}$ increases the affinity of ADP for its receptor, possibly via a $C_{60}(OH)_{24}$-dependent conformational change or via $C_{60}(OH)_{24}$-mediated inhibition of ticlopidine hydrochloride binding to P2Y12. Interestingly, $C_{60}(OH)_{24}$ did not affect collagen- or thrombin-induced platelet aggregation (data not shown). $C_{60}(OH)_{24}$ also failed to affect acetylsalicylic acid (aspirin)-mediated inhibition of collagen-induced aggregation, and RGDS peptide-mediated inhibition of thrombin-induced aggregation (data not shown). These results suggest that $C_{60}(OH)_{24}$ specifically stimulates ADP-induced platelet aggregation via an ADP receptor such as P2Y12, and that $C_{60}(OH)_{24}$ might contribute to thrombosis.

We used the ng/ml or μg/ml order concentration of CB and $C_{60}(OH)_{24}$ in experiments of macrophages. This concentration is similar to the maximal concentration of particulate matter <2.5 μm (PM2.5) in Chongqing, a city in China, ~700 $\mu g/m^3$ (daily average), and thus an individual might inhale 10,000 μg of particulate matter in a 24 h period. This is equivalent to approximately 1 μg/ml, considering that the extracellular fluid volume of a 60 kg individual is

12 L. However, the effective concentration of CB and $C_{60}(OH)_{24}$ was much higher than predicted physiological concentration in platelet experiments[12]

Taken together, the present results show that the effects of CB or $C_{60}(OH)_{24}$ on macrophage and platelet function contributes to cardiovascular diseases such as atherosclerosis, thrombosis and myocardial infarction. However, further experiments regarding the influence of nanomaterials on the cardiovascular system in vivo are required.

Acknowledgment

This study was supported by a Health and Labor Sciences Research Grant for Research on Risks of Chemical Substances (H17-chemistry-008 to N.I.) and a Grant-in-Aid for Scientific Research (#18590583 to Y.N.) from the Ministry of Education, Culture, Sports, Science and Technology of Japan.

References

1. Akerman ME, Chan WC, Laakkonen P, Bhatia SN, Ruoslahti E. Nanocrystal targeting in vivo. *Proc Natl Acad Sci USA* 2002; **99:** 12617–12621.
2. Borm PJ, Kreyling W. Toxicological hazards of inhaled nanoparticles–potential implications for drug delivery. *J Nanosci Nanotechnol* 2004; **4:** 521–531.
3. Kreuter J. Nanoparticulate systems for brain delivery of drugs. *Adv Drug Deliv Rev* 2001; **47:** 65–81.
4. Colvin VL. The potential environmental impact of engineered nanomaterials. *Nat Biotechnol* 2003; **21:** 1166–1170.
5. Oberdorster G, Oberdorster E, Oberdorster J. Nanotoxicology: An emerging discipline evolving from studies of ultrafine particles. *Environ Health Perspect* 2005; **113:** 823–839.
6. Jia G, Wang H, Yan L, Wang X, Pei R, Yan T, et al. Cytotoxicity of carbon nanomaterials: Single-wall nanotube, multi-wall nanotube, and fullerene. *Environ Sci Technol* 2005; **39:** 1378–1383.
7. Yamago S, Tokuyama H, Nakamura E, Kikuchi K, Kananishi S, Sueki K, et al. In vivo biological behavior of a water-miscible fullerene: 14C labeling, absorption, distribution, excretion and acute toxicity. *Chem Biol* 1995; **2:** 385–389.
8. Yamawaki H, Iwai N. Cytotoxicity of water-soluble fullerene in vascular endothelial cells. *Am J Physiol Cell Physiol* 2006; **290:** C1495–C1502.
9. Yamawaki H, Iwai N. Mechanisms underlying nano-sized air-pollution-mediated progression of atherosclerosis: Carbon black causes cytotoxic injury/inflammation and inhibits cell growth in vascular endothelial cells. *Circ J* 2006; **70:** 129–140.
10. Ozeki Y, Sudo T, Toga K, Nagamura Y, Ito H, Ogawa T, et al. Characterization of whole blood aggregation with a new type of aggregometer by a screen filtration pressure method. *Thromb Res* 2001; **101:** 65–72.
11. Monteil-Rivera F, Beaulieu C, Deschamps S, Paquet L, Hawari J. Determination of explosives in environmental water samples by solid-phase microextraction-liquid chromatography. *J Chromatogr A* 2004; **1048:** 213–221.
12. Radomski A, Jurasz P, Alonso-Escolano D, Drews M, Morandi M, Malinski T, et al. Nanoparticle-induced platelet aggregation and vascular thrombosis. *Br J Pharmacol* 2005; **146:** 882–893.
13. Brook RD, Franklin B, Cascio W, Hong Y, Howard G, Lipsett M, et al; Expert Panel on Population and Prevention Science of the American Heart Association. Air pollution and cardiovascular disease: A statement for healthcare professionals from the Expert Panel on Population and Prevention Science of the American Heart Association. *Circulation* 2004; **109:** 2655–2671.
14. Nemmar A, Hoet PH, Vanquickenborne B, Dinsdale D, Thomeer M, Hoylaerts MF, et al. Passage of inhaled particles into the blood circulation in humans. *Circulation* 2002; **105:** 411–414.
15. Nemmar A, Hoet PH, Dinsdale D, Vermylen J, Hoylaerts MF, Nemery B, et al. Diesel exhaust particles in lung acutely enhance experimental peripheral thrombosis. *Circulation* 2003; **107:** 1202–1208.
16. Peters A, Dockery DW, Muller JE, Mittleman MA. Increased particulate air pollution and the triggering of myocardial infarction. *Circulation* 2001; **103:** 2810–2815.
17. Bonetti PO, Lerman LO, Lerman A. Endothelial dysfunction: A marker of atherosclerotic risk. *Arterioscler Thromb Vasc Biol* 2003; **23:** 168–175.
18. Bosi S, Feruglio L, Da Ros T, Spalluto G, Gregoretti B, Terdoslavich M, et al. Hemolytic effects of water-soluble fullerene derivatives. *J Med Chem* 2004; **47:** 6711–6715.
19. Katsouyanni K, Touloumi G, Samouli E, Gryparis A, Le Tertre A, Monopolis Y, et al. Confounding and effect modification in the short-term effects of ambient particles on total mortality: Results from 29 European cities within the APHEA2 project. *Epidemiology* 2001; **12:** 521–531.
20. Dockery DW, Pope CA 3rd, Xu X, Spengler JD, Ware JH, Fay ME, et al. An association between air pollution and mortality in six U.S. cities. *N Engl J Med* 1993; **329:** 1753–1759.
21. Nemmar A, Hoet PH, Vermylen J, Nemery B, Hoylaerts MF. Pharmacological stabilization of mast cells abrogates late thrombotic events induced by diesel exhaust particles in hamsters. *Circulation* 2004; **110:** 1670–1677.
22. Libby P. Inflammation in atherosclerosis. *Nature* 2002; **420:** 868–874.
23. Ross R. Atherosclerosis--an inflammatory disease. *N Engl J Med* 1999; **340:** 115–126.
24. Manna SK, Sarkar S, Barr J, Wise K, Barrera EV, Jejelowo O, et al. Single-walled carbon nanotube induces oxidative stress and activates nuclear transcription factor-kappaB in human keratinocytes. *Nano Lett* 2005; **5:** 1676–1684.
25. Fratti RA, Chua J, Deretic V. Induction of p38 mitogen-activated protein kinase reduces early endosome autoantigen 1 (EEA1) recruitment to phagosomal membranes. *J Biol Chem* 2003; **278:** 46961–46967.
26. Sawamura T, Kume N, Aoyama T, Moriwaki H, Hoshikawa H, Aiba Y, et al. An endothelial receptor for oxidized low-density lipoprotein. *Nature* 1997; **386:** 73–77.
27. Chen M, Masaki T, Sawamura T. LOX-1, the receptor for oxidized low-density lipoprotein identified from endothelial cells: Implications in endothelial dysfunction and atherosclerosis. *Pharmacol Ther* 2002; **95:** 89–100.
28. Moriwaki H, Kume N, Kataoka H, Murase T, Nishi E, Sawamura T, et al. Expression of lectin-like oxidized low density lipoprotein receptor-1 in human and murine macrophages: Upregulated expression by TNF-alpha. *FEBS Lett* 1998; **440:** 29–32.
29. Kume N, Morikawa H, Kataoka H, Minami M, Murase T, Sawamura T, et al. Inducible expression of LOX-1, a novel receptor for oxidized LDL, in macrophages and vascular smooth muscle cells. *Ann N Y Acad Sci* 2000; **902:** 323–327.
30. Luttun A, Lutgens E, Manderveld A, Maris K, Collen D, Carmeliet P, et al. Loss of matrix metalloproteinase-9 or matrix metalloproteinase-12 protects apolipoprotein E-deficient mice against atherosclerotic media destruction but differentially affects plaque growth. *Circulation* 2004; **109:** 1408–1414.
31. Gough PJ, Gomez IG, Wille PT, Ranes EW. Macrophage expression of active MMP-9 induces acute plaque disruption in apoE-deficient mice. *J Clin Invest* 2006; **116:** 59–69.
32. Hollopeter G, Jantzen HM, Vincent D, Li G, England L, Ramakrishan V, et al. Identification of the platelet ADP receptor targeted by antithrombotic drugs. *Nature* 2001; **409:** 202–207.